Optics Communications 541 (2023) 129531

Contents lists available at ScienceDirect

Optics Communications

journal homepage: www.elsevier.com/locate/optcom

Aiming for high-capacity multi-modal free-space optical transmission leveraging complete modal basis sets

Zhouyi Hu [a], Yiming Li [a], Zhaozhong Chen [b], David M. Benton [a], Abdallah A.I. Ali [c], Mohammed Patel [a], Martin P.J. Lavery [b], Andrew D. Ellis [a,*]

[a] Aston Institute of Photonic Technology, Aston University, Birmingham, B4 7ET, UK
[b] James Watt school of engineering, University of Glasgow, Glasgow, G12 8QQ, UK
[c] Lumensisty Ltd, Unit 7, The Quadrangle, Abbey Park Industrial Estate, Romsey, SO51 9DL, UK

ARTICLE INFO

Dataset link: https://doi.org/10.17036/researchdata.aston.ac.uk.00000540

Keywords:
Free space optics
Optical communications

ABSTRACT

Free-space optical (FSO) communication has gained much interest due to its capability of providing not only a cost-efficient solution where the optical fiber is too expensive or too difficult to deploy but also a much higher system capacity than its radio-frequency competitor. In addition to conventional polarization-division multiplexing and coherent detection, combining with mode-division multiplexing can unlock the full potential of FSO communications and achieve ultra-high spectral efficiency. In this paper, we review the recent progress of multi-modal FSO communication systems leveraging complete modal basis sets. Some practical issues for system design are discussed. We also present two latest demonstrations that achieved the record-high single-wavelength data rate using a commercial transponder and a pair of commercial multiplexer/demultiplexer for multi-modal FSO transmission without turbulence and in atmospheric turbulence, respectively, showing the potential of such a technique.

1. Introduction

Although fiber optics plays a key role in modern communication technologies, it is not always cost-efficient to deploy optical fibers in sparsely-populated rural areas [1,2]. Traditionally, radio-frequency (RF) communications provide an alternate solution in these scenarios but are still facing some crucial challenges such as their low and licensed spectrum and relatively high power consumption. Free-space optical (FSO) communication, commonly referred to as optical wireless communication (OWC) working at 1300–1600 nm [3], therefore, is becoming a promising technique to deal with the above issues. However, the capacity and the maximal transmission distance of an FSO system are limited by atmospheric turbulence and various weather conditions such as fog and rain [4]. Therefore, extensive studies aiming to cope with these challenges have been reported for decades [5–10].

Meanwhile, to overcome the "capacity crunch" of optical networks, some researchers believe that space-division multiplexing (SDM) is the only option [11]. For FSO communications, SDM was first implemented by exploiting multiple light paths and detection with a detector array [12]. Nowadays, mode-division multiplexing (MDM) becomes an important subset. It is because MDM can provide multiple orthogonal and independent data-carrying optical beams to multiply the system capacity by the total number of transmit modes utilized. Meanwhile, since these orthogonal optical beams are still in the same wavelength range, the overall spectral efficiency can be increased, which is different from the other multiplexing techniques, such as time-division multiplexing (TDM) and wavelength-division multiplexing (WDM). Several modal basis sets have been used for MDM in FSO communications, among which orbital angular momentum (OAM) has been widely studied [13–19]. However, OAM is only a subset of Laguerre–Gaussian (LG) modes. By sacrificing its radial degrees of freedom, OAM has higher atmospheric turbulence resilience but would provide lower system capacity compared to other complete modal basis sets, e.g., LG modes, Hermite–Gaussian (HG) modes, and linearly polarized (LP) modes, for a given aperture size [20]. Therefore, these complete modal basis sets have attracted much attention in the last few years [21–27].

Despite the potential to further boost the system capacity, MDM-FSO systems leveraging complete modal basis sets still face some practical challenges. For example, as mentioned above, their transmission performance is more sensitive to the inherent inter-mode crosstalk of the multiplexer and demultiplexer as well as the influence of atmospheric turbulence. Although in a laboratory environment, the inter-mode crosstalk can be minimized by using a bulk-optics receiver typically comprising beam splitters and spatial light modulators (SLMs) [28,29], such a setup inevitably introduces very high insertion loss as the number of modes increases, which is not suitable for practical applications. Therefore, to optimize the overall system

* Corresponding author.
E-mail address: andrew.ellis@aston.ac.uk (A.D. Ellis).

https://doi.org/10.1016/j.optcom.2023.129531
Received 15 February 2023; Received in revised form 16 April 2023; Accepted 20 April 2023
Available online 26 April 2023

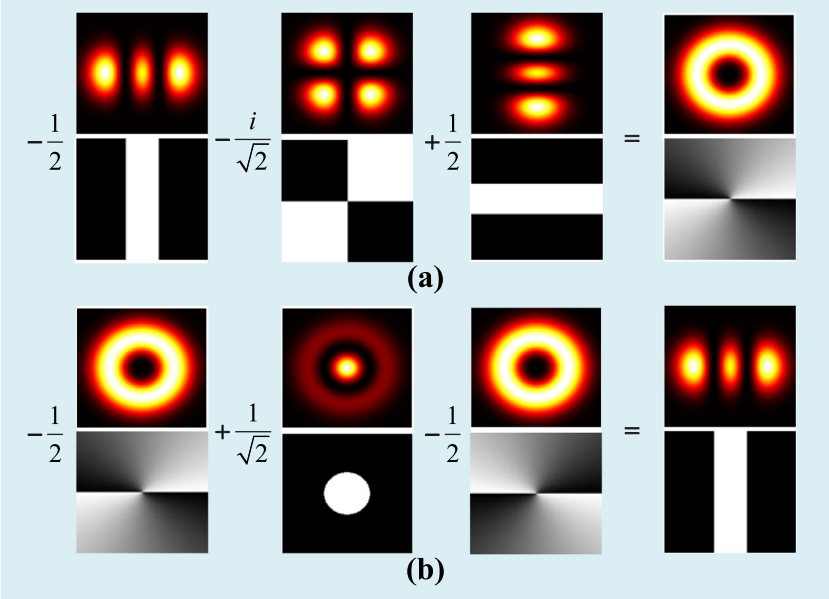

Fig. 1. Example (a) LG mode synthesis: $-(1/2) \times \mathrm{HG}_{2,0} - (i/\sqrt{2}) \times \mathrm{HG}_{1,1} + (1/2) \times \mathrm{HG}_{0,2} = \mathrm{LG}_{0,2}$ (first row: intensity distribution; second row: phase distribution), and (b) HG mode synthesis: $-(1/2) \times \mathrm{LG}_{0,2} + (1/\sqrt{2}) \times \mathrm{LG}_{1,0} - (1/2) \times \mathrm{LG}_{0,-2} = \mathrm{HG}_{2,0}$ (first row: intensity distribution; second row: phase distribution).

performance for practical MDM-FSO communications, from system impairments to the limit of the state-of-the-art commercial components are worthy of study.

In this paper, we review the recent trend and progress of multi-modal FSO communication systems leveraging complete modal basis sets. The impact of the FSO channel on system performance is discussed. We also discuss some practical issues related to the design of such a system, including devices and required digital signal processing (DSP) for the mitigation of system impairments. We then present our recently proposed schemes [30,31] for the implementation of high-capacity MDM-FSO transmission and compared them with other recent research results. Finally, we summarize the challenging issues in MDM-FSO communication using complete modal basis sets, and their potential solutions.

The rest of the paper is organized as follows. Section 2 discusses the complete modal basis set-based MDM-FSO communication systems. Section 3 summarizes recent high-speed MDM-FSO demonstrations. Section 4 discusses the practical issues for high-capacity MDM-FSO transmission and presents their potential solutions. Finally, Section 5 concludes this paper.

2. MDM-FSO communication leveraging complete modal basis sets

2.1. Modal basis sets

For the reader's convenience, we first provide a brief background of four widely used modal basis sets for MDM in optical communication systems. They are HG mode, LG mode, OAM mode, and LP mode.

1. *HG mode*: HG modes are the higher-order solutions to the paraxial wave equation in Cartesian coordinates, where the elementary solutions can be separated into products of identical solutions in the x and y directions. At position z, the solutions are given by [32]

$$u_{n,m}^{HG}(x,y,z) = \sqrt{\frac{2}{2^{(n+m)}\pi n!m!\omega_0^2}}\frac{q(0)}{q(z)}\left[-\frac{q^*(z)}{q(z)}\right]^{(n+m)/2} H_n\left[\frac{\sqrt{2}x}{\omega(z)}\right]H_m\left[\frac{\sqrt{2}y}{\omega(z)}\right]\exp\left[-\frac{x^2+y^2}{\omega^2(z)}\right]\exp\left[-\frac{ik\left(x^2+y^2\right)}{2R(z)}\right]\exp\left[i\psi_{n,m}(z)\right]\exp(-ikz), \quad (1)$$

where n and m are the mode indices corresponding to the x and y directions, respectively, $k = 2\pi/\lambda$ is the wave number (λ is the wavelength), ω_0 is the waist radius, $\omega(z) = \omega_0\left[1+\left(z/z_R\right)^2\right]^{1/2}$ is the radius of the beam at position z ($z_R = k\omega_0^2/2$ is the Rayleigh length), $q(z) = z + iz_R$ is the complex beam parameter, $R(z) = z\left[1+\left(z_R/z\right)^2\right]$ is the radius of curvature, $\psi_{n,m}(z) = (n+m+1)\tan^{-1}\left(\frac{z}{z_R}\right)$ is the Gouy phase shift, and $H_n(\cdot)$ and $H_m(\cdot)$ are the Hermite polynomials of order n and m, respectively.

2. *LG mode*: Different from HG modes, LG modes are the higher-order solutions in cylindrical coordinates. These solutions at position z are given by [32,33]

$$u_{p,l}^{LG}(r,\phi,z) = \sqrt{\frac{2p!}{\pi\omega^2(z)(p+|l|)!}}\left[\frac{r\sqrt{2}}{\omega(z)}\right]^{|l|}L_p^{|l|}\left[\frac{2r^2}{\omega^2(z)}\right]\exp\left[-\frac{r^2}{\omega^2(z)}\right]\exp\left[-\frac{ikr^2}{2R(z)}\right]\exp(-il\phi)\exp\left[i\psi_{p,l}(z)\right]\exp(-ikz), \quad (2)$$

where p and l are the radial mode index and the azimuthal mode index, respectively, $\psi_{p,l}(z) = (2p+|l|+1)\tan^{-1}\left(\frac{z}{z_R}\right)$ is the Gouy phase shift, and $L_p^{|l|}$ is the generalized Laguerre polynomial. It should be noted that LG modes can be expressed as the sum of HG modes and vice versa [34], as illustrated in Fig. 1. Meanwhile, for the conventional single-input single-output (SISO) FSO communication system, usually only the fundamental Gaussian beam, i.e., $\mathrm{HG}_{00}/\mathrm{LG}_{00}$ mode, is transmitted. In this case, however, the mode itself is not detected or used for carrying independent data.

3. *OAM mode*: Various beams can carry OAM, including LG beams [33], Bessel beams [35], Mathieu beams [36], and Ince-Gaussian beams [37], among which LG beams are probably the most widely known [38]. In this case, OAM modes can be described by a subset of LG modal basis set without the radial degree of freedom, i.e., $p = 0$ in Eq. (2) [20,39,40], yielding

$$u_l^{OAM}(r,\phi,z) = \sqrt{\frac{2}{\pi\omega^2(z)|l|!}}\left[\frac{r\sqrt{2}}{\omega(z)}\right]^{|l|}\exp\left[-\frac{r^2}{\omega^2(z)}\right]\exp\left[-\frac{ikr^2}{2R(z)}\right]\exp(-il\phi)\exp\left[i\psi_l(z)\right]\exp(-ikz), \quad (3)$$

where $\psi_l(z) = (|l|+1)\tan^{-1}\left(\frac{z}{z_R}\right)$.

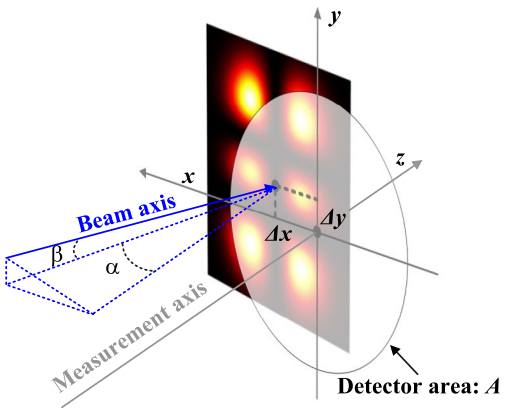

Fig. 2. Illustration of detection with pointing error in MDM-FSO (HG_{12} mode received) systems. The beam axis is tilted with respect to the angle α and β in the x-z and y-z planes, respectively. The lateral displacements are Δx and Δy, respectively.

Therefore, only the azimuthal index l is responsible for the OAM, indicating the rate of azimuthal twist of the phase front [27,41]. Since for each value of l, different from OAM modes, LG modes can utilize an infinite number of p values as independent data-carrying beams in theory, OAM would provide lower system capacity for a given aperture than LG modes as well as other complete mode sets.

4. *LP mode*: LP mode set in two polarizations is complete and can be used to represent fiber modes in the weakly guiding approximation. Considering a cylindrically symmetric fiber, the field distribution is given by [42,43]

$$u_{l,p}^{LP}(r,\phi,z) = C_{l,p}^{LP}\begin{cases}\dfrac{J_l\left(\frac{\upsilon_{lp}r}{a}\right)}{J_l\left(\upsilon_{lp}\right)}\exp(-il\phi)\exp(-ikz) & \text{for } r<a\\ \dfrac{K_l\left(\frac{\mu_{lp}r}{a}\right)}{K_l\left(\mu_{lp}\right)}\exp(-il\phi)\exp(-ikz) & \text{for } r\geq a\end{cases}, \tag{4}$$

where $C_{l,p}^{LP}$ is a normalization constant, a is the core radius of fiber, J_l denotes the lth order Bessel-function of the first kind, K_l denotes the lth order modified Bessel-function of the second kind, $\upsilon_{l,p}$ is the normalized propagation constant of the core, and $\mu_{l,p}$ is the normalized propagation constant of the cladding. It should be noted that although LP modes are excited in a weakly guiding step-index fiber, they can be approximated by a scale-adapted set of the aforementioned LG free-space modes [42].

2.2. FSO channel impairments

We then summarize the major channel impairments that should be taken into account for high-capacity multi-modal FSO transmission.

1. *Atmospheric attenuation* : A laser beam is absorbed and scattered by particles when it propagates through a medium such as the atmosphere in FSO systems, leading to atmospheric attenuation that can be described by the exponential Beers–Lambert Law as

$$h_a(z) = \frac{P(z)}{P(0)} = \exp(-\gamma(\lambda)z), \tag{5}$$

where $P(z)$ is the optical power at position z, and $\gamma(\lambda)$ is the wavelength (λ) -dependent attenuation coefficient. Table 1 summarizes some typical values of the visibility range and the attenuation under different atmospheric conditions [4].

2. *Geometric loss and pointing errors* : Another factor causing attenuation is the geometric spread with pointing error when the receiver aperture cannot fully capture the received laser beam [44–46]. As illustrated in Fig. 2, the major factors affecting the performance of the received MDM beam include lateral displacements donated by Δx and Δy, angular errors denoted by α and β, and truncation due to limited receiver aperture size, where the detector area is denoted by A. Take

Table 1
Visibility range and atmospheric attenuation under different weather conditions.
Source: Adapted with permission from [4] © The Optical Society.

Atmospheric condition	Visibility (km)	Attenuation (dB/km) at 850 nm	Attenuation (dB/km) at 1550 nm
Clear air	23	0.42	0.2
Haze	4	2.8	1.6
Mist	2	6	4
Light fog	1	13	9
Moderate fog	0.5	28	21
Dense fog	0.2	73	60
Heavy fog	0.05	309	272

for example the HG modes. The complex amplitude of the misaligned HG_{nm} beam is [45]

$$u_{n,m}^{HG,Mis}(x,y,z) = u_{n,m}^{HG}(x-\Delta x, y-\Delta y, z)\exp[ik(x\sin(\alpha)+y\sin(\beta))], \tag{6}$$

The attenuation due to limited receiver aperture size is then expressed as

$$h_{n,m}^{HG,Mis}(z) = \frac{\iint_{x,y\subset A} u_{n,m}^{HG,Mis}(x,y,z)\,u_{n,m}^{HG,Mis,*}(x,y,z)\,dxdy}{\iint_{\infty} u_{n,m}^{HG,Mis}(x,y,z)\,u_{n,m}^{HG,Mis,*}(x,y,z)\,dxdy}, \tag{7}$$

It should be noted that the radius of the beam at position z, i.e., $\omega(z)$, is spread after propagation due to both beam divergence and atmospheric turbulence [47], leading to increased power loss. Meanwhile, since MDM is a subset of SDM, the lateral and angular misalignment due to pointing errors also results in mode-dependent loss (MDL) and inter-mode crosstalk [21,45–48]. Let HG_{nm} be the transmit mode, and $HG_{n'm'}$ be the mode to be coupled after the receiver aperture. Then, the mode coupling efficiency between two modes due to misalignment and limited aperture size is [49–52]

$$\eta_{n,m-n',m'}^{HG,Mis}(z) = \frac{\left|\iint_{x,y\subset A} u_{n,m}^{HG,Mis}(x,y,z)\,u_{n',m'}^{HG,*}(x,y,z)\,dxdy\right|^2}{\iint_{\infty} u_{n,m}^{HG,Mis}(x,y,z)\,u_{n,m}^{HG,Mis,*}(x,y,z)\,dxdy \iint_{\infty} u_{n',m'}^{HG}(x,y,z)\,u_{n',m'}^{HG,*}(x,y,z)\,dxdy}, \tag{8}$$

In this work, we compared the mode coupling of LG modes and HG modes as a function of lateral displacement, angular error, and divergence after propagation, respectively, as shown in Figs. 3–5. For a fair comparison, all three modes (LG_{11}, HG_{12}, HG_{12}) considered as the transmit mode have the same order of the beam, i.e., $n+m=2p+|l|$. The beam waist ω_0 is 1 cm. The receiver aperture is circular, with a diameter of 4 cm. When studying lateral displacement and angular error, the back-to-back (B2B) transmission was assumed.

For Fig. 4(c) and 5(c), we can see that HG_{12} mode and HG_{21} mode have the same curve for beam divergence. It is because they are symmetric and share the same intensity distribution after a 90-degree rotation. Meanwhile, when we compare the modal coupling of LG modes and HG modes for different link lengths (Fig. 3(c) vs. 4(c) and 5(c)), we can observe that LG modes are more robust against a limited-size receiver aperture in terms of power loss, which can be attributed to their circular profile and the circular detection aperture assumed in this work. From Fig. 4(a)–(b) and 5(a)–(b), we can also note that compared to HG_{21} mode, HG_{12} mode has a higher tolerance to the horizontal (x-axis) displacement as well as the angular error in x-z plane due to the narrower intensity distribution of HG_{12} mode along the x-axis, as illustrated in Fig. 2.

In MDM-FSO systems, there is a transition from free space to fiber and vice verse. Therefore, inter-mode crosstalk and MDL also occur during the mode coupling between free-space modes and fiber modes [42]. Similar to the aforementioned receiver aperture, the fiber coupling efficiency would also be reduced due to the fiber positioning error (e.g., lateral displacement, defocus, and fiber tilt) as well as atmospheric turbulence [53–55]. Meanwhile, the incomplete modal overlap between free-space modes and fiber modes, e.g., the transition between

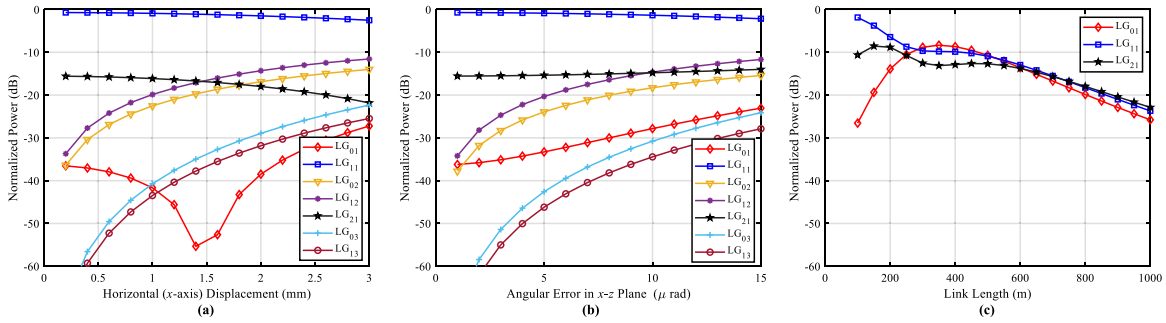

Fig. 3. Simulated power distribution among different LG modes as function of (a) horizontal (x-axis) displacement (B2B), (b) angular error in x-z plane (B2B), and (c) link length. Only LG_{11} mode is transmitted. The beam waist ω_0 is 1 cm. The receiver aperture is circular, with a diameter of 4 cm. For the link length ≥50 m, the normalized power of LG_{02}, LG_{12}, LG_{03} and LG_{13} is always below −60 dB.

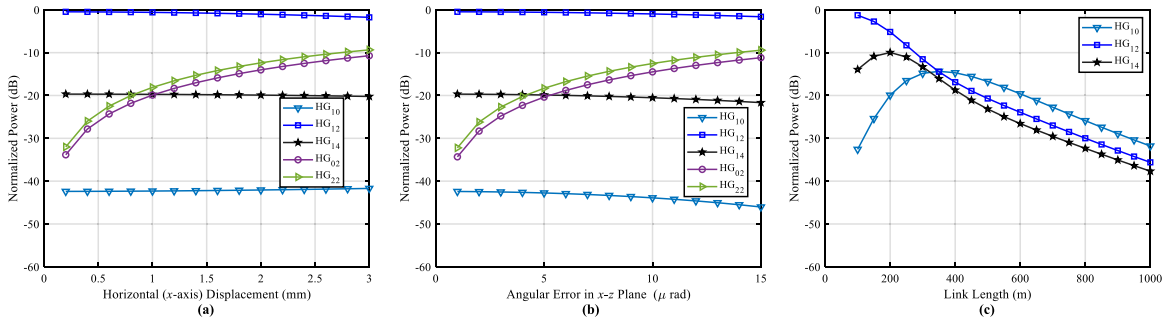

Fig. 4. Simulated power distribution among different HG modes as function of (a) horizontal (x-axis) displacement (B2B), (b) angular error in x-z plane (B2B), and (c) link length. Only HG_{12} mode is transmitted. The beam waist ω_0 is 1 cm. The receiver aperture is circular, with a diameter of 4 cm. For the link length ≥50 m, the normalized power of HG_{02} and HG_{22} is always below −60 dB.

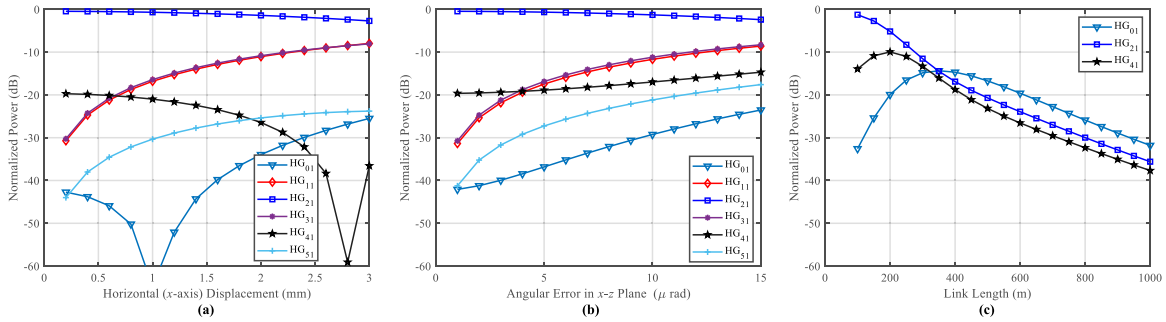

Fig. 5. Simulated power distribution among different HG modes as function of (a) horizontal (x-axis) displacement (B2B), (b) angular error in x-z plane (B2B), and (c) link length. Only HG_{21} mode is transmitted. The beam waist ω_0 is 1 cm. The receiver aperture is circular, with a diameter of 4 cm. For the link length ≥50 m, the normalized power of HG_{11} and HG_{31} is always below −60 dB.

LG modes and LP modes [42], is another major factor resulting in the coupling loss.

3. *Atmospheric turbulence*: Turbulence is another primary atmospheric phenomenon that affects optical wave propagation. It is a result of random temperature variations and convective processes in atmosphere, which aberrates the wavefront of the laser beam. The classical theory of turbulence was developed in the early 1940s by Kolmogorov who related these temperature fluctuations to refractive index fluctuations [56]. In the Kolmogorov mode, two boundary values specify the average size of turbulent cells, i.e., the inner (small) scale l_0, and the outer (large) scale L_0. When we assume $l_0 = 0$ and $L_0 = \infty$, the power spectral density (PSD) of refractive index fluctuation can be described by the Kolmogorov power-law spectrum as [57]

$$\Phi_n(\kappa) = 0.033 C_n^2 \kappa^{-11/3}, 1/L_0 \le \kappa \le 1/l_0. \tag{9}$$

where C_n^2 is the refractive index structure parameter whose typical values range between 10^{-17} $m^{-2/3}$ and 10^{-13} $m^{-2/3}$ as turbulence increases from weak to strong [58], and κ is a spatial frequency coordinate.

When inner scale and/or outer scale effects cannot be ignored, a more general form called the modified von Kármán spectrum is used, which is described by

$$\Phi_n(\kappa) = 0.033 C_n^2 \exp\left(-\frac{\kappa^2}{\kappa_m^2}\right)\left(\kappa^2 + \kappa_0\right)^{-11/6}, 0 \le \kappa < \infty, \tag{10}$$

where $\kappa_m = 5.92/l_0$ and $\kappa_0 = 2\pi/L_0$ (or sometimes $\kappa_0 = 1/L_0$) [57].

Instead of C_n^2, turbulence strength is often specified using the Fried parameter r_0 and the Strehl Ratio (SR), which are described in Eqs. (11) and (12), respectively, as [57,59]

$$r_0 = \left(0.42 C_n^2 Z k^2\right)^{-3/5}, \tag{11}$$

$$\mathrm{SR} = \frac{\langle I_{\mathrm{beam}}(0,Z)\rangle}{I^0_{\mathrm{beam}}(0,Z)} \cong \frac{1}{\left[1 + \left(D_G/r_0\right)^{5/3}\right]^{6/5}}, \tag{12}$$

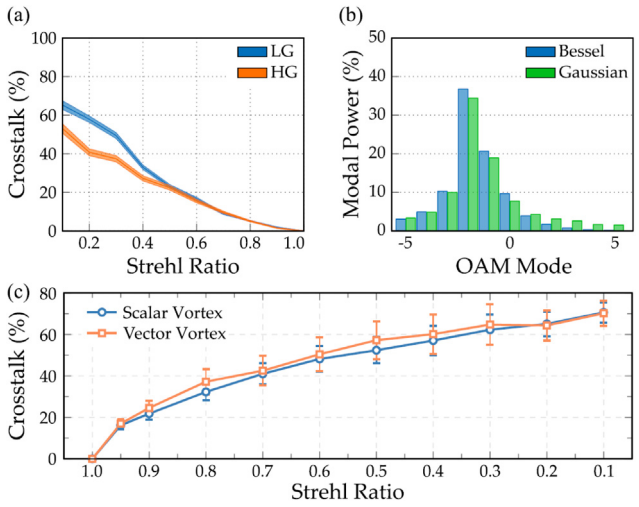

Fig. 6. (a) Crosstalk for HG and LG modes in turbulence characterized by SR showing that HG modes exhibit lower crosstalk in strong turbulence. (b) Long range Bessel modes versus a Gaussian in weak turbulence over 150 m showing lower losses for the Bessel beam. (c) Scalar versus vector vortex modes [23].

where Z is the path length, D_G is the aperture diameter, and $\langle I_{\text{beam}}(0,Z)\rangle$ and $I^0_{\text{beam}}(0,Z)$ are the on-axis mean irradiance in turbulence of a point source and that in the absence of turbulence, respectively. Other methods, such as Zernike modes, can also be used to represent wavefront distortions of optical beams in turbulence [60].

In FSO systems, atmospheric turbulence not only leads to random and time-variant fluctuations in intensity but also beam wander as well as geometric spread discussed above. Specifically, the radius of the beam after propagating in atmospheric turbulence can be approximated as [47]

$$\omega(z) = \omega_0 \left[1 + \varepsilon \left(\frac{\lambda z}{\pi \omega_0^2}\right)^2\right]^{\frac{1}{2}}, \tag{13}$$

$$\varepsilon = 1 + 2\left[\frac{\omega_0}{\left(0.55 C_n^2 k^2 z\right)^{-3/5}}\right]^2. \tag{14}$$

We can notice from Eqs. (10) and (11) that when the effect of turbulence can be neglected, we have $\varepsilon \to 1$. Then the beam waist is increased only because of beam divergence. However, when turbulence cannot be neglected, it becomes an additional factor of beam spread.

Since atmospheric turbulence aberrates the wavefront of the laser beam, in an MDM-FSO system, this channel impairment also induces inter-mode crosstalk as well as MDL, reducing the overall system capacity. Compared to incomplete modal basis sets, the complete modal basis sets that support more modes for a given aperture size are potentially more sensitive to such degradation [41,61,62]. Even for complete modal basis sets, since different sets have different characteristics and symmetries, they may have basis-dependent performance in turbulence. In a recent study by M. A. Cox et al. [23], the authors compared the resilience of different sets of spatial modes to turbulence as presented in Fig. 6. Results in Fig. 6(a) show that in strong turbulence, HG modes (low order and excluding the symmetrical HG_{11} case) are significantly more robust than LG modes. Meanwhile, we can see from Fig. 6(b) that when considering long distance propagation for FSO communications, Bessel beams outperform Gaussian beams in atmospheric turbulence in terms of power delivery. It is because Bessel beams have higher resistance to spreading as it propagates [23,63,64]. The crosstalk as a function of turbulence strength, quantified by SR, for scalar and vector vortex modes is also illustrated in Fig. 6(c), showing that there is no performance benefit in using vector modes over scalar modes in terms of crosstalk due to turbulence [65].

2.3. System design

Various factors should be taken into account when we develop a high-capacity MDM-FSO system. For example, although ultra-high speed demonstrations beyond 1 Pb/s [66] have been reported in a laboratory study, performance is not the only metric for system design. From the implementation perspective, other issues such as the portability for commercial applications should also be considered.

1. *Types of FSO systems* : Similar to RF wireless systems, based on the number of transmitters and receivers, FSO systems can be classified as SISO, single-input multi-output (SIMO), multi-input single-output (MISO), and MIMO systems, as illustrated in Fig. 7(a)–(d), respectively. Multi-aperture systems are used as an example but can be easily transformed into multi-mode systems. SISO systems require the fewest resources among all four types but are not as robust as SIMO or MISO systems, or capable of providing ultra-high spectral efficiency as MIMO systems. In SIMO and MISO systems, the spatial (multi-aperture system) or modal (multi-aperture system) diversity can be utilized to increase the robustness of the FSO system against channel impairments, e.g., the turbulence discussed above [9,49,67–69]. This is because separated paths or different spatial modes experience turbulence differently, which provides additional information for diversity. However, both schemes sacrifice their capabilities to use many modes for carrying more information content. Therefore, full MIMO-FSO systems leveraging mode-based multiplexing techniques, i.e., MDM-FSO systems, become a promising solution to overcome the capacity crunch nowadays.

In a SISO-FSO system, usually, only the fundamental Gaussian beam is generated for carrying data at the transmitter. Although after FSO propagation, the received beam may not maintain as a pure Gaussian beam due to channel impairments such as turbulence, the detector only captures the light without any spatial mode discrimination. Therefore, all of the impairments only affect the transmission performance in terms of the power budget [70]. In a SIMO system with modal diversity, the power coupled to higher-order modes due to channel impairments provides the capability of receive diversity [49,67,68], which shares a similar mechanism with spatial diversity reception leveraging a detector array [71]. With the help of a diversity combining algorithm, e.g., selective combining, maximal-ratio combining and equal gain combining, the SIMO-FSO system can achieve higher tolerance to turbulence and other channel impairments compared to SISO systems [49,71,72]. MISO systems can also increase the resilience of an FSO link by transmitting many different spatial modes at the transmitter side, while being detected by a single receiver. As we discussed earlier in Section 2.2, different spatial modes experience channel impairments differently, and therefore can provide modal diversity. Meanwhile, it was found that multiple modes with the same mode order but from different modal basis sets can also achieve a diversity gain in a MISO-FSO system [69]. When the same data is transmitted, MIMO-FSO systems can simultaneously employ transmit and receive diversity [73], reducing error probability in FSO channels with turbulence [74]. It should be noted that modal and spatial diversity can be employed together in a MIMO-FSO system to further improve turbulence resiliency [75]. In a MIMO MDM-FSO system, however, the multiplexing technique is used to boost the system capacity, where the inter-channel crosstalk is desired to be eliminated after MIMO detection. Therefore, in this case, channel impairments affect the transmission performance in terms of not only the power budget but also the MDL and crosstalk, i.e., the condition number of the MIMO transfer function matrix [76]. Conventionally, the receive modes used for reception are the same as the transmit modes in an MDM-FSO system [21,77], where the number of receive modes (N_r) is the same as the number of transmit modes (N_t). Although resources can be minimized, the system is sensitive to the inter-mode crosstalk induced by either devices or turbulence, easily leading to ill-conditioning. Therefore, in our recent works [30,31,78–80], we have generalized our MIMO MDM-FSO system to support

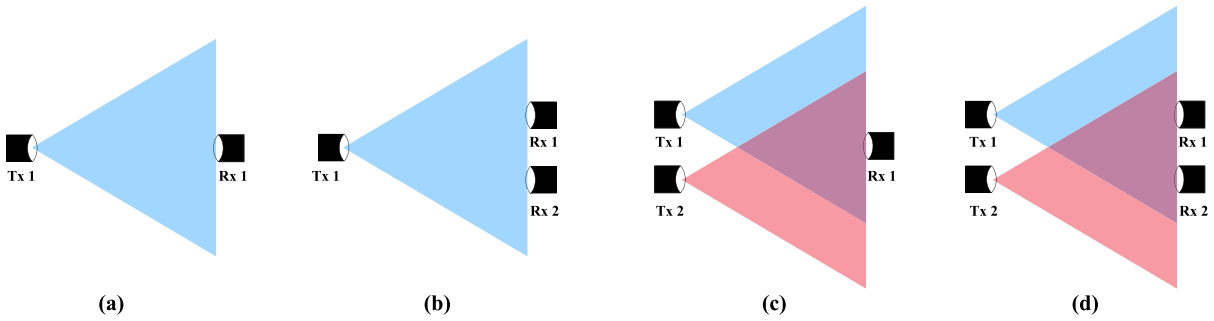

Fig. 7. Various types of FSO systems: (a) SISO; (b) SIMO; (c) MISO; (d) MIMO. Multi-aperture systems are used for illustration. When spatial modes are used for multiplexing or diversity, the physical separation is in the form of orthogonal spatial modes instead of separated paths.

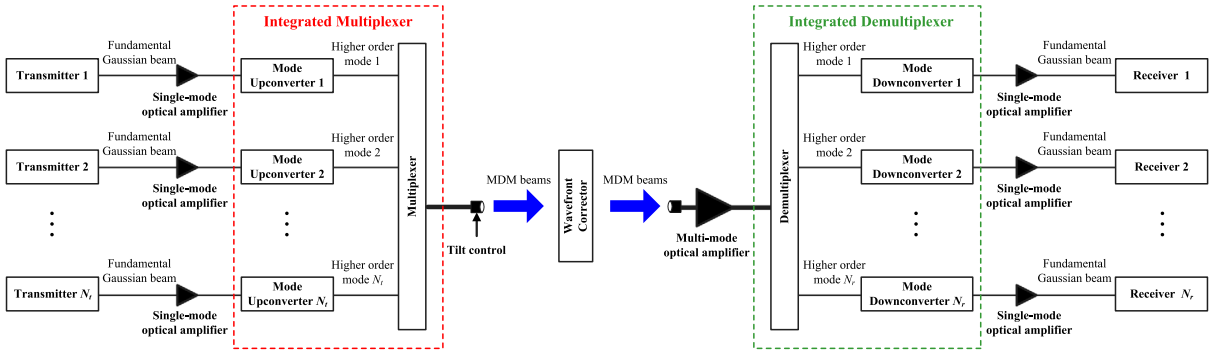

Fig. 8. Illustration of a typical MDM-FSO system.

redundant receive modes, i.e., $N_r \geq N_t$, for robust MDM-FSO transmission, which provides a compromise between transmission performance and requirements for resources.

2. *Devices* : Required devices for a typical MDM-FSO system are illustrated in Fig. 8. Besides the conventional devices such as laser sources, collimators, single-mode optical amplifiers, and photodiodes, an MDM-FSO system needs additional mode converter and multiplexer/demultiplexer for MDM implementation, which is different from SISO-FSO systems. A multi-mode optical amplifier can also be employed immediately after the receiver fiber collimator to improve the robustness against turbulence in an MDM-FSO system [68,81]. Meanwhile, different from fiber systems, acquisition, tracking, and pointing (ATP) mechanisms for the minimization of pointing errors, and adaptive optics (AO) for wavefront correction are also required for the implementation of high-speed MDM-FSO transmission.

The major difference between single-mode and MDM-FSO systems is that MDM-FSO systems should be capable of converting fundamental Gaussian beams to higher-order modes, and vice versa. As shown in Fig. 8, this function is usually followed by multiplexing, leading to an integrated device of the multiplexer in practical applications [82]. Since a pair of multiplexer and demultiplexer can induce additional MDL, inter-mode crosstalk, and insertion loss, which have significant impacts on the transmission performance, this device is important for the design of a high-capacity MDM-FSO system. Binary phase plate converters [83] used to be widely studied due to their simplicity. However, their large intrinsic insertion loss limited their practical application [84]. At present, although the diffractive-optic approach leveraging SLMs or digital micro-mirror devices (DMD) has been widely used for mode conversion in the laboratory [17], which has already been applied to various modal basis sets, such as OAM, LG, and HG modes [13,21,85], these types of devices are too bulky and costly for commercial implementation. From the implementation perspective, photonic lanterns and multi-plane light conversion (MPLC) devices are the most promising technologies [86] to simultaneously multiplex all modes with relatively low insertion loss as well as cost. Meanwhile, there are already some commercial products of photonic lanterns [87] and MPLC [88], demonstrating their applicability. Fig. 9 depicts the schematics of fused fiber photonic lanterns and MPLC devices. As shown in Fig. 9(a), photonic lanterns consist of a single-mode end and a multi-mode end, which are interfaced through a physical waveguide transition, i.e., the capillary tube shown in the figure. The capillary tube has a lower refractive index than the single-mode fibers (SMFs). Therefore, when the SMF cores nearly vanish, the SMF cladding becomes the new multi-mode core, and the low-index capillary becomes the multi-mode fiber cladding. By properly making the starting SMF cores dissimilar, the resultant different propagation constants of the initial guided modes can be utilized to implement mode selectivity, i.e., the so-called mode-selective photonic lanterns [89]. Since photonic lanterns are directly spliced to fibers, they can achieve sub-dB insertion losses and broadband mode selectivity. Therefore, photonic lanterns have been considered the best choice for MDM up to ten spatial modes by some researchers [82]. However, due to fabrication challenges, photonic lanterns are not easy to scale to very large mode counts (e.g., >100 modes). MPLC, therefore, becomes an alternative solution. As shown in Fig. 9(b), using multiple phase planes instead of a single plane can convert an orthogonal set of input modes into a completely different orthogonal set of output modes. Since the spatial multiplexing that transforms one mode basis into another mode basis can be considered as a spatial unitary transform, there is a succession of phase profiles that can achieve the desired unitary transform based on optical Fourier transforms in theory [90]. In practical applications, the phase mask design for each phase plate can be optimized numerically [91]. We can note that the insertion loss of MPLC is determined by the number of phase planes required. The first generation of MLPC requires the same order of the number of spatial modes [92]. Fortunately, with the help of a 2D configuration, the spatially separated Gaussian beams can be converted to HG modes using a much smaller number of planes. A design supporting 1035 HG modes has been demonstrated using only 14 phase planes [93]. LG modes can also be obtained with additional HG-LG conversion [91]. Table 2 compares photonic lanterns and MPLC

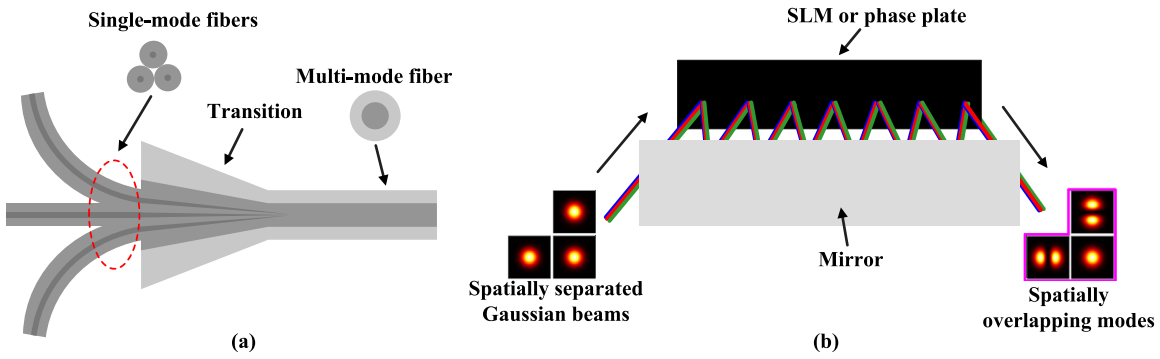

Fig. 9. Schematics of (a) photonic lantern and (b) MPLC.

Table 2
High-level comparison of photonic lanterns and MPLC [82].

Device	Best application	Scalability	Fabrication maturity	Loss	Bandwidth	Size
Photonic lantern	Low loss and broadband	100s of fibers	Labor intensity	<1 dB	100–500 nm	A few cm long
MPLC	Complex modes	1035 HG modes	Wafer-scale	>3 dB	100 nm	100 mm^3 to 10 cm^3

at a high level [82]. It should be noted that although photonic lanterns are fiber-based devices, spatial modes for FSO communications can still be generated with appropriate modification. For example, it has been demonstrated that OAM modes can be generated by a modified photonic lantern with an annular refractive index profile [94]. On the other hand, although MPLC has been prototyped using SLM in many studies, it is not cost-efficient for commercial implementation [92]. Therefore, lithographically etching fixed phase masks are probably the best choice for practical applications [82].

Multi-mode optical amplifier is another exciting area of research, which can potentially provide huge cost savings over single-mode amplifiers through spatial integration. Multi-mode optical amplifiers have been developed by different methods, including doped fibers [95], Raman pumping [96], and semiconductors [97]. Although they are fiber-based devices, it has been demonstrated that the multi-mode optical amplifier can still significantly improve the turbulence resiliency of an MDM-FSO system by pre-amplification of the turbulent beams as soon as it is collected [68,81]. The major challenge of multi-mode optical amplification is minimizing the mode-dependent gain (MDG) induced by the amplifier [86]. Several schemes have been proposed to deal with this issue. Take for example the multi-mode erbium-doped fiber amplifiers (EDFAs). The MDG can be minimized by optimizing the erbium doping concentration profile [98–100] or shaping the launched pump light [101–103]. However, further scaling of the number of modes would need complex fiber fabrication strategies and/or system implementations when using these techniques. Therefore, cladding pumping using high-power multi-mode pump diodes becomes a promising solution to cope with this challenge [104]. By adopting an intentionally oversized doped core to improve the confinement of low-order mode groups and maximizing the overlap of each mode with the gain medium, the side-pump coupling with the cladding pumping scheme can already support 36 spatial modes, 16-dB gain and 25-dBm output power across the C-band with only <0.5-dB differential modal gain [105]. Meanwhile, there are already some commercially available products, e.g., the few-mode EDFA manufactured by Phoenix Photonics Ltd [106] . Based on the results in our previous work [78], the few-mode EDFA induced an optical signal-to-noise ratio (OSNR) penalty of more than 1.5 dB compared to the B2B case.

In practical FSO applications, collimation is required. As we discussed earlier in Section 2.2, the pointing error caused by the misalignment of transceivers and the beam wander from turbulence is a major FSO channel impairment. It not only induces power losses but also additional MDL and inter-mode crosstalk when MDM is employed. Therefore, as shown in Fig. 8, acquisition, tracking, and pointing (ATP) mechanisms for collimator tilt control are required to minimize such degradation in a high-capacity MDM-FSO system. Meanwhile, the effect of wavefront distortions caused by atmospheric turbulence is another factor limiting the transmission performance. To minimize such an effect, wavefront correction usually implemented by adaptive optics (AO) is employed before the reception as shown in Fig. 8. It should be noticed that AO can be classified as a type of ATP system [107]. ATP mechanisms can be classified based on their working principles and mechanics, i.e., gimbal-based, mirror-based, gimbal-mirror hybrid, AO, liquid crystal, RF-FSO hybrid, and other ATP Mechanisms [107]. Fig. 10(a) depicts an example two-axis gimbal for ATP, which can perform pan and tilt rotations with a mirror mounted on the gimbal [107]. This type of ATP mechanism stands out from all ATP options mentioned above due to its low complexity and low cost allied to a wide field of view [108]. However, it shows limited precision (microradians) when compared with other schemes such as AO systems (nanoradians). AO is a technology that can correct wavefront distortions caused by atmospheric turbulence as illustrated in Fig. 10(b). An AO system typically consists of AO elements (wavefront corrector) for wavefront correction, a wavefront sensor for the estimation of the impact of turbulence, and an AO controller for the control of the AO elements based on the feedback messages from the wavefront sensor. The wavefront corrector can be built by an array of deformable mirrors, liquid crystals (SLM), a DMD, or a simple tip/tilt mirror to only correct the lower-order aberrations of turbulence. Since an AO system is able to compensate for aberrations in a complex optical system and partially undo the modal coupling, it is particularly useful for the MDM-FSO systems that suffer from atmospheric turbulence [109,110].

3. *DSP:* Although all-optical signal processing needs much less power than with DSP [86,111], DSP is still required in most scenarios for its high flexibility as well superior performance. Especially for achieving ultra-high capacity, complex coherent optical systems and complete modal basis sets are suggested. In that case, the use of DSP to maximize transmission performance is inevitable. In addition to the conventional DSP (e.g., Nyquist-pulse shaping, timing recovery, and frequency-offset estimation) required in a SISO system, MDM-FSO also needs additional DSP of multi-input multi-output (MIMO) demultiplexing (or called MIMO detection) to unscramble the inter-mode crosstalk due to the imperfection of multi-modal devices (e.g., demultiplexer and multi-mode optical amplifier) and the effect of atmospheric turbulence. It should be noted that since turbulence is time-variant, adaptive algorithms are usually desired. When inter-symbol interference (ISI) due to impulse response also exists, it is necessary to eliminate both the ISI and the inter-mode crosstalk. Although it has been demonstrated

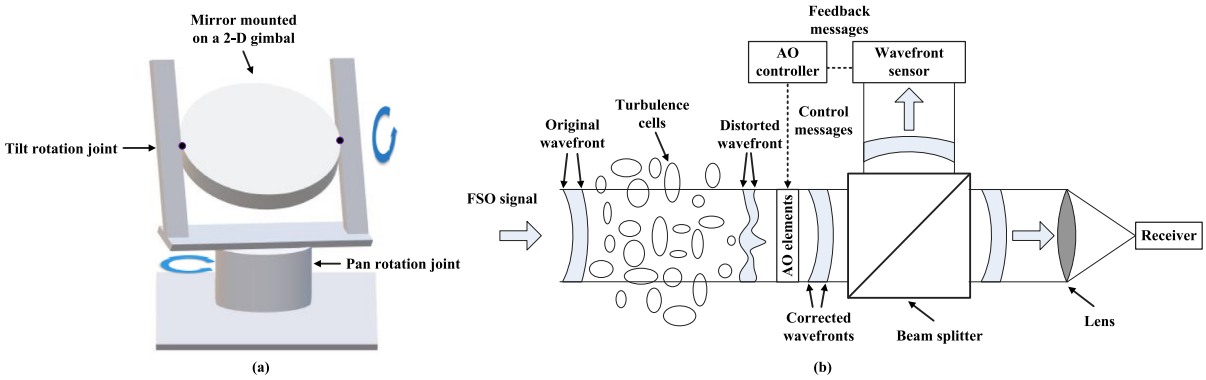

Fig. 10. Schematics of (a) a two-axis gimbal, and (b) an AO system for turbulent FSO links.

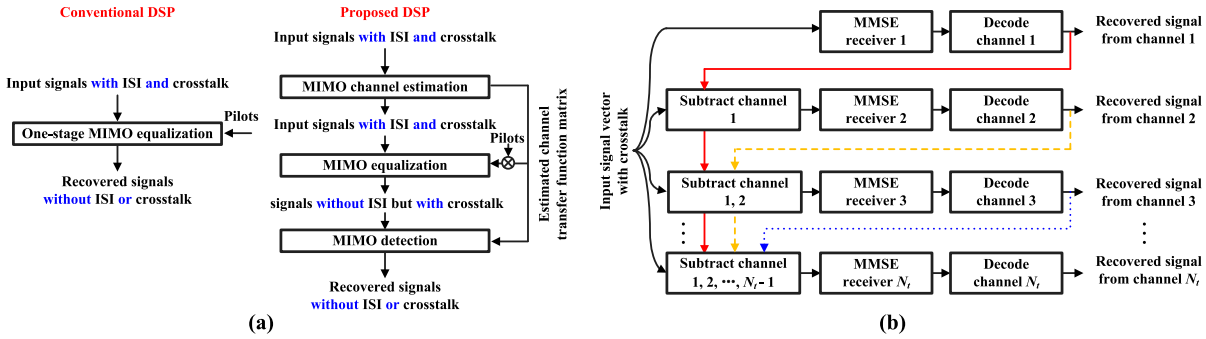

Fig. 11. (a) Comparison of the conventional one-stage MIMO equalization and the proposed three-stage process. (b) Schematic diagram of the SIC algorithm.

that a one-stage MIMO equalizer can compensate for both the impulse response and the exchange of power between modes in a fiber-based MDM optical system [112], such a DSP algorithm inevitably leads to noise amplification in a non-unitary channel, e.g., MDM-FSO systems with power loss (or MDL). To handle this issue, we proposed to divide this one-stage process into three stages as shown in Fig. 11(a). They are MIMO channel estimation, MIMO equalization, and MIMO detection [30,31,78–80]. We can see from the figure that the conventional one-stage MIMO equalization cancels ISI and crosstalk simultaneously by optimizing toward an objective function of the transmitted pilot sequence, while the MIMO equalization in the proposed three-stage process only targets the impulse response by a modified objective function that is the estimated channel matrix from the first stage acting on the known pilot sequence. This modified objective function clearly does not equalize the mode mixing, but instead compensates for the impact of the channel memory. This stage is then followed by an independent memoryless MIMO decoder that can suppress such noise amplification by leveraging an advanced detection algorithm, such as minimum mean-squared error (MMSE), successive interference cancellation (SIC), and maximum likelihood detection (MLD) [113]. MMSE has the lowest complexity among the above three algorithms, but is still vulnerable to a nonunitary channel. MLD is the optimal MIMO detection algorithm, but has an extremely high computational complexity that is exponential in the number of transmitters (N_t) and the order of the modulation format. Meanwhile, SIC is one of the most popular detection algorithms for MIMO systems, which can achieve suboptimal performance, but much lower complexity compared to MLD, leading to better portability for practical applications. As shown in Fig. 11(b) [31], the main idea of SIC is successively canceling out the interference of the best channel from the remaining channels using decoded bits and the estimated channel matrix. In our recent works [31], we have demonstrated that SIC can significantly improve the transmission performance of an MDM-FSO system compared to the MMSE decoder in the scenario with atmospheric turbulence.

DSP can also be employed at the transmitter side for the implementation of high-capacity MDM-FSO transmission. Due to the different conditions experienced by the signals from different transmitters, they have different signal-to-noise ratios (SNRs) after transmission. To maximize the throughput of the system, the modulation formats and power can be optimally allocated to different transmit modes based on the pre-estimated channel state information (CSI) with an adaptive loading algorithm [114,115]. In our recent works [80], we have demonstrated that combining adaptive loading and more powerful MIMO decoders can bring on transmission performance improvement when suffering from strong turbulence, not only compared to the conventional scheme without adaptive loading and with simple MMSE detection, but also the scheme only with adaptive loading or only with powerful MIMO decoders. However, the CSI applied to the transmitted signal is determined from an earlier pilot, as determined by the processing delays and the channel round trip time. If the channel fluctuations (e.g., atmospheric turbulence) are more rapid than this timescale, inaccuracy of the estimated CSI can result in degradation of the adaptive loading scheme. In a ground-to-ground FSO communication system, if we consider a typical wavelength of 1550 nm, typical turbulence ($C_n^2 = 1.7 \times 10^{-14}\,\mathrm{m}^{-2/3}$), and a wind velocity of 21 m/s, and compare the Greenwood time constant [116,117] to the round trip time of the link, it is easy to show that the maximum link length is ~10 km. For a low earth orbit satellite-to-ground FSO system, even with a 0-degree zenith angle, the corresponding Greenwood time constant is ~4 ms [118] leading to a maximum link length of ~60 km, precluding the use of receiver-directed adaptive loading as well as other CSI-based precoding algorithms in FSO MIMO satellite applications.

3. Demonstrations of high-capacity MDM-FSO transmission

In this section, we first introduce a novel time-division multiplexed (TDM) experimental setup for the demonstration of MDM-FSO systems in a laboratory environment (Section 3.1). With only one coherent

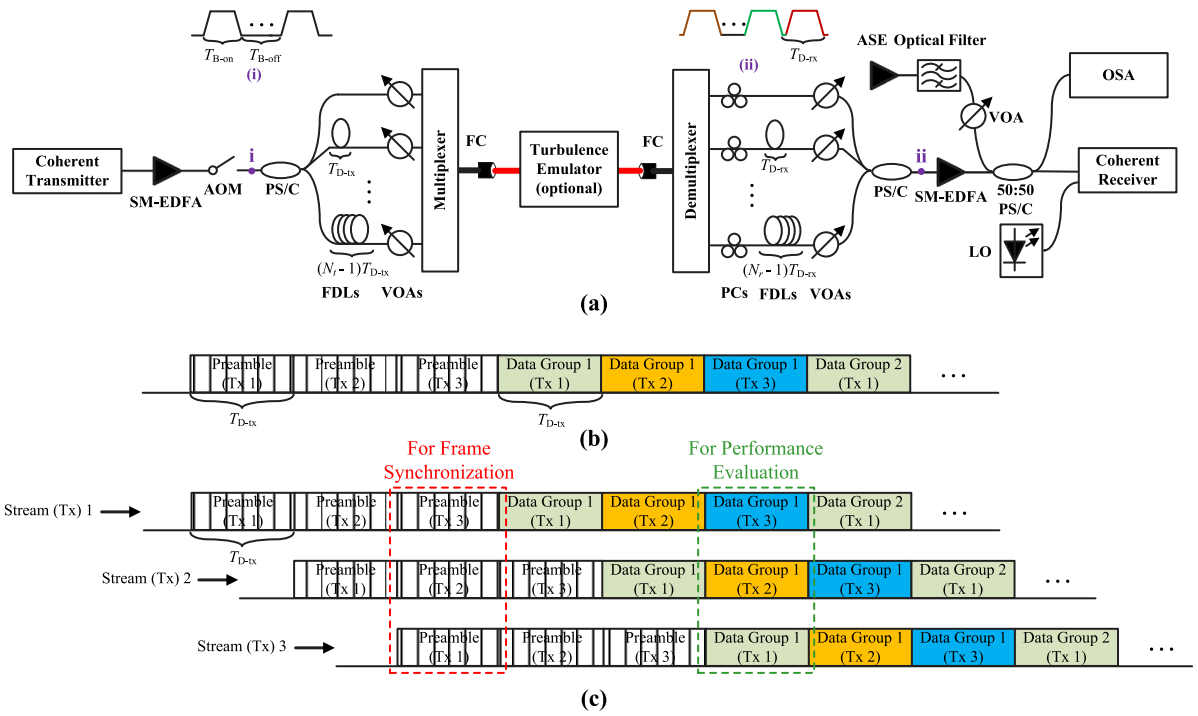

Fig. 12. (a) Generalized TDM experimental setup for the emulation of a full MIMO MDM-FSO systems (AOM, acousto-optic modulator; ASE, amplified spontaneous emission; FC, fiber collimator; FDL, fiber delay line; LO, local oscillator; OSA, optical spectrum analyzer; PC, polarization controller; PS/C, power splitter/coupler; VOA, variable optical attenuator); Insets: (i) signal bursts after AOM; (ii) TDM signal bursts after interleaving. Example TDM signals (b) written to the transponder, and (c) after the power splitter and transmitter FDLs, respectively, where $N_t = 3$ for illustration.

transmitter and one coherent receiver, such a setup can emulate a full MIMO system with channelized precoding schemes, greatly saving experimental resources. We then review our recent demonstrations (Sections 3.2 and 3.3) of high-capacity MDM-FSO transmission in both the cases without turbulence (emulation of the indoor environment) and with turbulence (emulation of the outdoor environment). To demonstrate good practical applicability, all key devices, including multiplexer/demultiplexer and coherent transponder, are commercially available. In Section 3.4, we also review other recent representative high-capacity FSO demonstrations.

3.1. TDM experimental setup

Fig. 12(a) shows the generalized TDM experimental setup for MDM-FSO demonstrations. Fig. 12(b) and (c) illustrate the proposed TDM frames to enable channelized precoding schemes, where only 3 transmitters are shown for illustration. As shown in Fig. 12(b), each frame written to the transponder comprised a preamble with a time duration of $T_{\mathrm{D-tx}}$ for each transmit mode to enable frame synchronization, followed by a repeating structure of cascaded data groups (also $T_{\mathrm{D-tx}}$ long) with data rotating through the channels. The TDM signals generated from the coherent transmitter are then amplified by a single-mode optical amplifier before being gated by an acousto-optic modulator (AOM). As shown in Inset (i) of Fig. 12(a), the gate width and the gate period are set to $T_{\mathrm{B-on}}$ and $T_{\mathrm{B-on}} + T_{\mathrm{B-off}}$, respectively, and should guarantee a duty cycle $T_{\mathrm{B-on}}/\left(T_{\mathrm{B-on}} + T_{\mathrm{B-off}}\right)$ smaller than $1/N_r$ to allow room for a block per mode at the receiver. After passing through a power splitter and an array of variable fiber delay lines (FDLs), the preambles and data groups are time aligned, but delayed by $\left(n_t - 1\right) T_{\mathrm{D-tx}}$, where $n_t = 1, 2, \ldots, N_t$. Therefore, as shown in Fig. 12(c), the preambles and data groups representing different transmitters are aligned for frame synchronization where all training symbols are aligned (highlighted in red) or performance evaluation where all transmitter payloads are aligned in the correct order (highlighted in green) at the receiver side. It should be noted that for an N_t-transmitter system to be emulated, $1/N_t$ of the groups comprise the originally intended data patterns. An array of variable optical attenuators (VOA) are employed to balance any transmitter-side MDL, after which a multiplexer (e.g., MPLC or photonic lantern) is used for MDM implementation. MDM optical signal is then launched into free space through a fiber collimator (FC). An optional turbulence emulator can be used to impose the effects of turbulence on the optical signal. This device could be an SLM [31], a phase plate [119], a digital micromirror device [120], etc.

At the receiver side, another FC is used to couple the light into the multi-mode fiber. The MDM signal is then demultiplexed by a demultiplexer. The resultant N_r streams, one per mode, are delayed by another array of FDLs with an incremental delay of $T_{\mathrm{D-rx}}$ and then combined to produce a TDM stream of successive $T_{\mathrm{B-on}}$ bursts of frames corresponding to the detected signal from each mode. To avoid overlap, we have $T_{\mathrm{D-rx}} > T_{\mathrm{B-on}}$. These are optically amplified, noise loaded, and detected by a single coherent receiver where the $T_{\mathrm{D-rx}}$ delays are digitally reversed, this whole process emulating N_r independent receivers. Before combination of the streams, an array of polarization controllers (PCs) is employed along with another array of VOAs to minimize the impact of quantization noise from analog-to-digital conversion. The interleaved signal is illustrated in Inset (ii) of Fig. 12(a). The OSNR of the interleaved signal is measured by an optical spectrum analyzer (OSA) and represents an average OSNR over all modes. The signal is finally detected by a single coherent receiver with a local oscillator (LO).

3.2. Single-wavelength terabit MDM-FSO transmission

With the help of the proposed TDM setup presented above, in our recent work [30], we demonstrated a record-high net single-wavelength data rate of 1.1 Tbit/s and net spectral efficiency of 28.35 bit/s/Hz using a commercial transponder and multiplexer for turbulence-free FSO transmission. To demonstrate good practical applicability, a pair of commercial six-mode mode-selective photonic lanterns (Phoenix Photonics, Ltd.) were employed in our experiment, where Fig. 13 shows

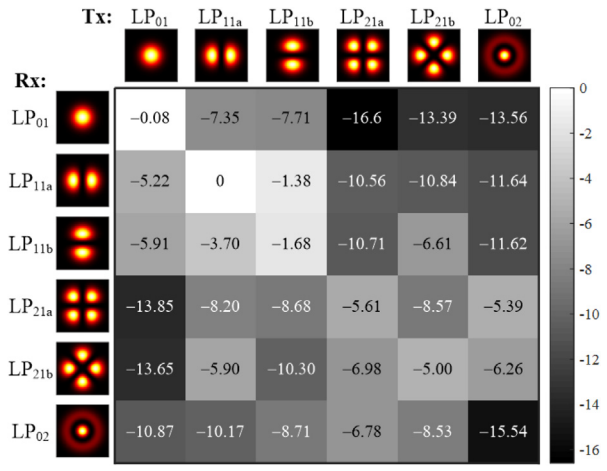

Fig. 13. Measured crosstalk matrix (dB) of the pair of mode-selective photonic lanterns, normalized to LP_{11a}.
Source: Reprinted with permission from [30] ©The Optical Society.

the measured normalized crosstalk matrix of the pair of them. As we can see from the figure, the LP modes were excited with relatively large inter-mode crosstalk. At the transmitter side, we used a commercial Ciena Wave WaveLogic 3 transponder with a sampling rate of 39.385 GSa/s and a laser wavelength of 1550.12 nm for optical signal generation. Dual-polarization quadrature amplitude modulation (DP-QAM) with or without adaptive loading was used for performance comparison. The signal was also Nyquist-shaped with a roll-off factor of 0.05 before transmission. For TDM frame structure and signal burst, we set T_{D-tx} to 8.12 ns, T_{D-rx} to 24.5 μs, T_{B-on} to 20 μs, and T_{B-off} to 140 μs. The overall overhead included pilot overhead of 10%, framing overhead of 2%, and HD-FEC overhead of 6.25% [121]. The FSO link was ~1 m. At the receiver side, a standard coherent receiver with a 50-GSa/s sampling rate and 23-GHz bandwidth real-time oscilloscope was employed for reception and the subsequent offline DSP. We used a simple MMSE decoder for MIMO detection in this work.

We first compared the transmission performance of the MDM signals with and without adaptive loading as shown in Figs. 14(a) and 14(b). For a fair comparison, the data rate of all signals was fixed at 885 Gbit/s by allocating 30 bits across all 10 channels (2 polarizations × 5 modes) and setting the symbol rate to 29.5 Gbaud. To verify the feasibility of the robust reception using all six receive modes, we also evaluated the performance of the MDM-FSO system with only the first five receive modes. We can see from Fig. 14(a) that both adaptive loading and one more receiver can bring on OSNR sensitivity improvement at the hard-decision forward error correction (HD-FEC) threshold of 4.7×10^{-3} [121]. The performance improvement from adaptive loading can be explained by Fig. 14(b). In the case without adaptive loading, the bit-error rate (BER) of different channels shows a very large fluctuation due to the difference in SNR in our MIMO system. Meanwhile, this problem can be effectively solved by allocating different modulation formats and power to different channels based on the SNR estimated before transmission [115]. The average BER is thus reduced from 6.28×10^{-3} to 1.56×10^{-3}, meeting the requirement of HD-FEC.

We finally maximized the throughput of our MDM-FSO system by leveraging adaptive loading, as shown in Fig. 14(c). Herein, we varied the number of transmitters and the total number of bits allocated. The number of receivers was fixed at six, except the case with five transmitters and five receivers was attached as the benchmark. The symbol rate was set to 36.9 Gbaud for all cases. We can see from the figure that by enabling the first five modes for carrying data, we successfully achieved a maximum line rate of ~1.33 Tbit/s (≈36 *bits* × 36.9 Gbaud). After considering all overhead, the net data rate and the net spectral efficiency achieved in this work were ~1.1 Tbit/s/wavelength and 28.35 bit/s/Hz, respectively, which were both record-high when all key devices were commercially available for turbulence-free MDM-FSO transmission.

3.3. High-capacity MDM-FSO transmission over turbulence link with SIC DSP

We have also experimentally demonstrated a high-capacity MDM-FSO system with SIC DSP to combat turbulence [31]. The demonstration was also based on the TDM setup shown in Fig. 12 where the turbulence was emulated by an SLM, and the related part is depicted in Fig. 15(a). We can see from Fig. 15(a) that the collimated light was passed through the SLM twice to modulate both polarization components of the MDM-FSO signal. Simulated phase screens were displayed on the left and right half of the SLM. During the first pass, the horizontal polarization component was modulated by the turbulence phase screen. A half-wave plate (HWP) located in-between the first and second passes swapped the horizontal and vertical components. And then the unaffected component in the first pass was modulated by the same turbulence phase screen during the second pass. Figs. 15(b) and 15(c) show the typical (half) patterns written to the SLM for the emulation of stronger turbulence ($r_0 = 0.8$ mm) and weaker turbulence ($r_0 = 3.0$ mm), respectively.

Same as the turbulence-free demonstration introduced in Section 3.2, we employed the pair of commercial six-mode mode-selective photonic lanterns for multiplexing and demultiplexing, the commercial Ciena WaveLogic 3 transponder for optical signal generation, and the same standard coherent receiver and real-time oscilloscope for reception. Meanwhile, for implementing the TDM receiver, T_{D-tx}, T_{D-rx}, T_{B-on}, and T_{B-off} were still set to 8.12 ns, 24.5 μs, 20 μs and 140 μs, respectively. The uniform DP-4-QAM symbols with a fixed symbol rate of 34.46 Gbaud were Nyquist-shaped with a roll-off factor of 0.1 before transmission. The overall overhead included pilot overhead of 10%, framing overhead of 8.4%, and HD-FEC overhead of 6.25%. The SLM for turbulence emulation had 1920 × 1152 pixels, where the size of each pixel was 9.2 × 9.2 μm^2. For the FSO link, it was 50 cm between FC and SLM, 50 cm between mirror and SLM, and 20 cm between two mirrors. We set the inner scale (l_0) and the outer scale (L_0) to 0.1 mm and 10 m, respectively. The Fried parameter (r_0) was set to 3.0 mm and 0. 8 mm for emulating weaker and stronger turbulence, respectively. The diameter of the receiver lens (D_G) was 8.4 mm in this work. For the receiver-side DSP, MMSE and SIC decoders were used for performance comparison.

We first examined the BER performance against the average OSNR of the MDM-FSO signal with 5 transmit modes and 6 receive modes under different turbulence conditions, as shown in Fig. 16. We can see from Fig. 16(a) that for a turbulence-free situation, SIC system has a 2.2 dB implementation penalty compared to the theory curve at the HD-FEC limit, which can be attributed to the inter-mode crosstalk and residual MDL in the photonic lantern pair. These imperfections have a slightly higher impact on the MMSE system (2.7 dB implementation penalty). Nevertheless, the performance difference between SIC and MMSE decoders increases with increasing turbulence. In order to better understand the enhanced turbulence resiliency by the proposed SIC system, Fig. 16(b) depicts the BER of the best channel (with minimum BER), the worst channel (with maximum BER), and the average BER of all channels (also shown in Fig. 16(a)) in the stronger turbulence. The best channels in both the SIC system and the MMSE system have similar BER performance, this is because we did not execute any interference cancellation for the first decoded channel in the SIC system as shown in Fig. 11(b). On the other hand, the worst channel in the SIC system has a much better performance than it in the MMSE system. This is because a higher effective signal-to-interference-plus-noise ratio can be achieved in the SIC system by canceling out the previously decoded channels. Considering the fact that the worst channel is the dominant factor in

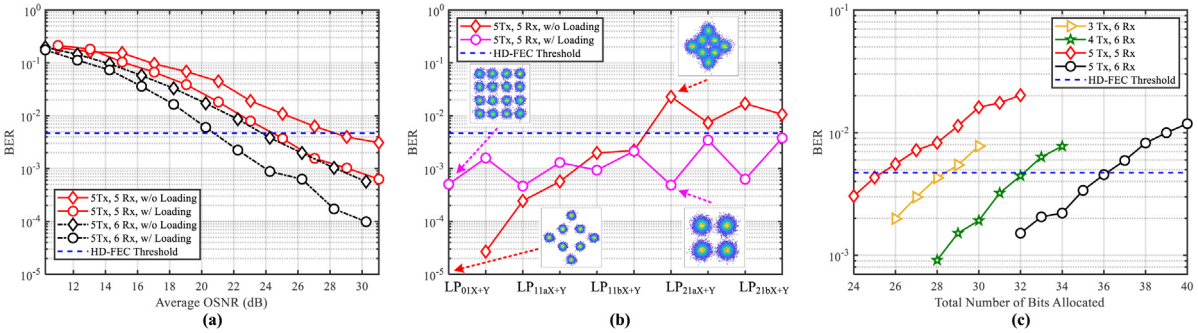

Fig. 14. (a) Transmission performance of different signals at the same data rate (30 bits, 29.5 Gbaud). (b) BER versus channel index for the signals with and without adaptive loading (30 bits, 29.5 Gbaud, average OSNR = 27.04 dB). (c) Throughput maximization with adaptive loading and different schemes (36.9 Gbaud) for turbulence-free MDM-FSO transmission.
Source: Reprinted with permission from [30] © The Optical Society.

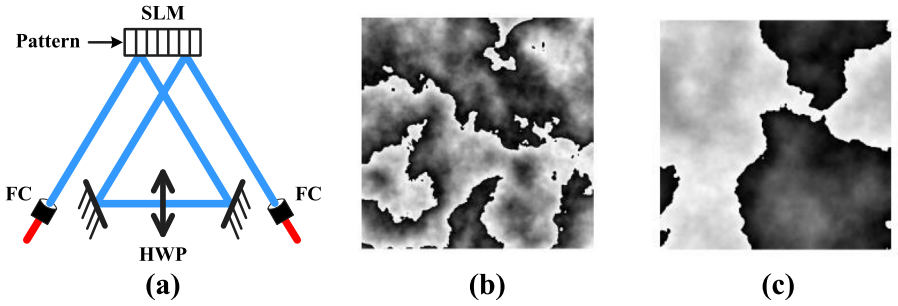

Fig. 15. (a) Turbulence emulator based on SLM. Typical patterns of (b) stronger turbulence ($r_0 = 0.8$ mm), and (c) weaker turbulence ($r_0 = 3.0$ mm), respectively.

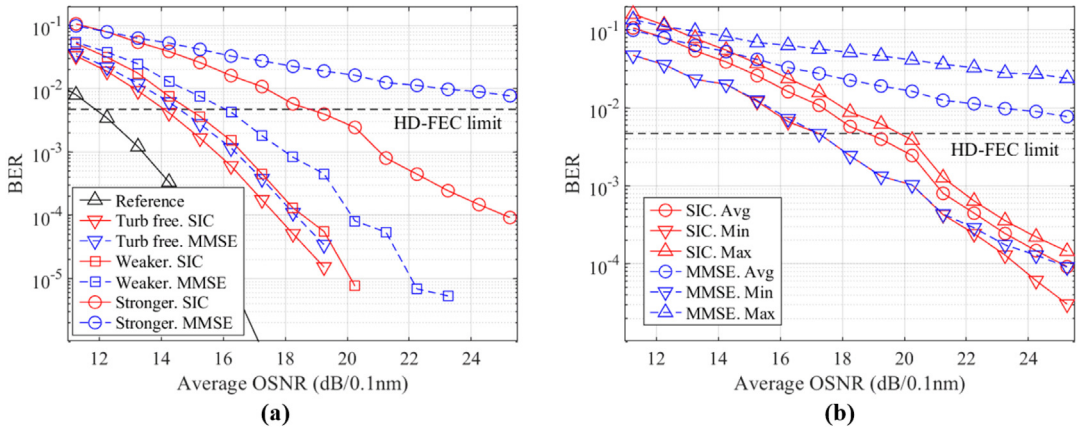

Fig. 16. (a) Average BER curves of the MDM-FSO system ($N_t = 5$, $N_r = 6$) under different turbulence intensities ($r_0 = 3.0$ mm for weaker turbulence, $r_0 = 0.8$ mm for stronger turbulence). Reference: Theoretical reference curve in an ideal system. (b) BER curves of the MDM-FSO system ($N_t = 5$, $N_r = 6$) under strong turbulence.
Source: Adapted with permission from [31] © IEEE.

the average BER performance, the SIC system can obtain a significantly lower average BER in turbulent channels.

We then tested 120 independent turbulence patterns under the stronger turbulence case without noise loading. As shown in Fig. 17(a), the BER of the SIC system is consistently lower than the MMSE system. As a result, the average BER among different turbulence realizations is decreased by an order of magnitude from 8.02×10^{-3} in the MMSE system to 4.76×10^{-4} in the SIC system. The probability distribution of the BER in Fig. 17(a) is depicted in Fig. 17(b) for better clarity. If we consider an outage when the BER is larger than the HD-FEC limit, we have an outage probability of 48.3% in the MMSE system and only 2.5% in the SIC system, suggesting a more robust transmission using SIC.

In Fig. 18, we also compared the transmission performance of different transmit and receive mode numbers in turbulence, where the average BER is calculated using 120 independent patterns under the strong turbulence case without noise loading. The results indicate that both SIC and increasing the number of receive modes can enhance atmospheric turbulence resiliency.

In this work, we successfully demonstrated a record-high independent channel number of 10 and a line rate of 689.23 Gbit/s in strong turbulence. After considering all overhead, a record-high net spectral efficiency of 13.9 b/s/Hz was also achieved over emulated turbulent MDM FSO links.

3.4. Recent representative demonstrations

In Table 3, besides our recent works, we summarized some of the recent representative high-capacity FSO demonstrations. It should

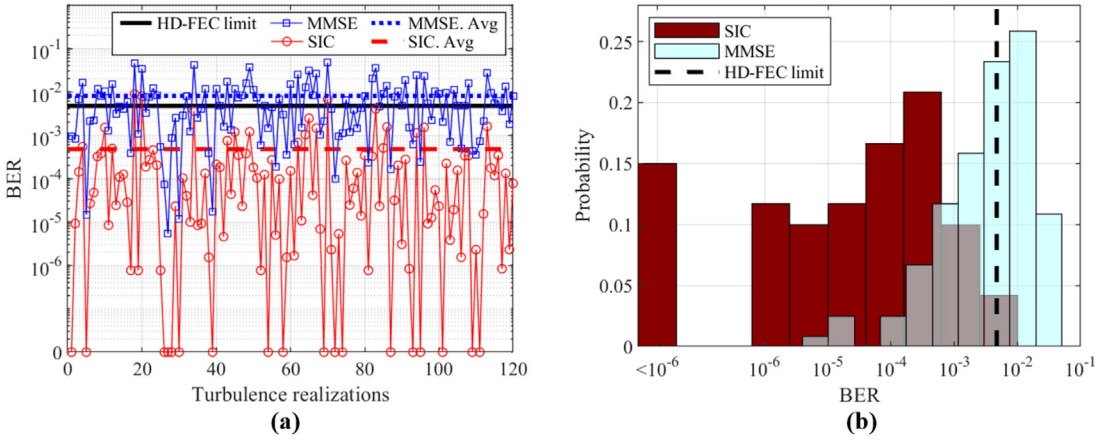

Fig. 17. (a) The BER performance of the MDM-FSO system ($N_t = 5$, $N_r = 6$) under 120 stronger turbulence realizations, and (b) its probability distribution.
Source: Adapted with permission from [31] © IEEE.

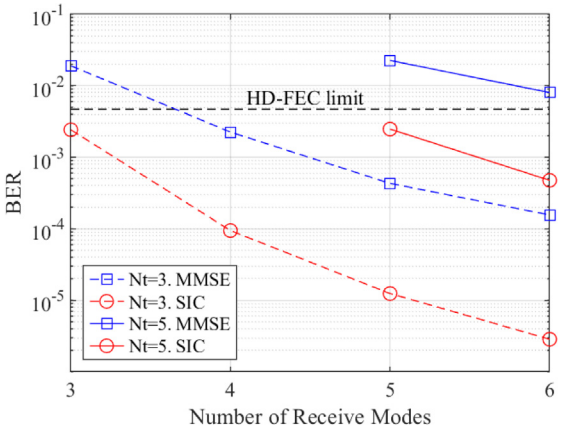

Fig. 18. The average BER performance of different MIMO systems under 120 stronger turbulence realizations.
Source: Adapted with permission from [31] © IEEE.

be noted that not only MDM-FSO systems but also some demonstrations based on the conventional SISO (single mode) FSO system have been selected for a more comprehensive comparison. In [66], a very high aggregate transmission capacity of 1.036 Pb/s and spectral efficiency of 112.6 bit/s/Hz have been reported in a turbulence-free laboratory environment by employing 26 OAM modes and 368 wavelengths. However, in this work, all channels were only divided into two groups, where each group of channels was modulated by the same data, leading to incomplete decorrelation as well as underestimated inter-mode crosstalk in practical applications. The longest-range MDM-FSO communication field demonstration to date was reported in [122], where two OAM modes were employed for achieving an aggregate data rate of 80 Gb/s and successfully transmitted over a 260-m FSO link with real atmospheric turbulence, although some farther propagation has been studied without data transfer [123,124]. Results show that atmospheric turbulence is a significant challenge for long-reach MDM-FSO transmission. Fortunately, its negative effects can be mitigated by either AO or DSP methods, which will be discussed later in Section 4. Particularly in a laboratory environment, a long-distance turbulent FSO channel can be simulated by SLMs, where the optical path can also be scaled down to more manageable lengths while maintaining the Fresnel number to simulate an equivalent distance in practical FSO propagation [125]. Besides popular OAM modes, since both modal indices can be utilized to achieve a larger potential orthogonal modal space, complete modal basis sets such as HG modes and LG modes have attracted much attention in the last few years. In [21], a 400-Gb/s FSO communication link has been experimentally demonstrated by leveraging four HG modes or four LG modes. Meanwhile, the crosstalk performances of these two modal bases under different misalignments have been studied in this work.

Besides using spatial modes for multiplexing, there have been several SIMO-FSO demonstrations leveraging multiple modes for robust transmission in turbulence [49,126]. Although most current studies only achieved low data rates, the improved performance compared to the single-mode reception indicates the potential of using modal diversity for high-capacity FSO transmission.

For SISO-FSO systems, the single-wavelength terabit transmission was first reported in [127], where adaptive probabilistic constellation shaping was utilized to approach the capacity limit. Impressively, in 2022, a 1-Tb/s 53 km single wavelength FSO link was demonstrated outdoors [70]. With the help of an AO system, the impact of atmospheric turbulence can be significantly mitigated.

As an important competitor of MDM, WDM which can multiply the single-wavelength data rate by the number of wavelengths is another promising technology to achieve ultra-high throughput in FSO systems. In 2018, researchers from the German Aerospace Center (DLR) demonstrated an aggregated line rate of 1.72 Tb/s over a 10.45 km WDM-FSO link with on–off-keying (OOK) modulation [128]. In the not-too-distant 2019, the aggregate line was further increased to 13.16 Tb/s by using DP-QAM formats and coherent detection [129]. Compared to MDM, WDM is more mature, especially in fiber-optic networks [132]. Fortunately, in FSO systems, there are no long-distance SMFs needed to be replaced with few-mode fibers, leading to simpler and cheaper implementation. Although WDM can provide an ultra-high aggregated data rate via wideband transmission, it is not able to increase the spectral efficiency of the whole system, which is very different from the MDM scheme. Furthermore, WDM and MDM are not mutually exclusive and can be therefore combined to further boost the system capacity, e.g., the demonstration in [66]. It should be noted that polarization-division multiplexing (PDM) is usually included in coherent optical systems with both WDM and MDM technologies, e.g., our recently reported high-speed FSO demonstrations [30,31] introduced above.

Meanwhile, different from MDM-FSO systems, there are already some commercial products for single-mode FSO systems. For example, the highest data rate that a commercial system can support is 30 Gb/s with a reach distance of 1.3 km [130], while the longest range of a commercial FSO link is up to 5 km at a data rate of 10 Gb/s [131].

From Table 3, we can see that although SISO-FSO systems can also achieve an ultra-high data rate, their spectral efficiency is still much

Table 3
Recent representative demonstrations of high-capacity FSO transmission.

Institute	Line rate[a]	FSO link length	Modal basis	No. of Tx modes	No. of λ	Spectral efficiency	Environment	Remark
HUST [66]	1.036 Pb/s	Not reported	OAM	26	365	112.6 bit/s/Hz	Turbulence-free	Incomplete decorrelation; underestimated crosstalk
AiPT [30]	1.33 Tb/s	1 m	LP	5	1	34.3 bit/s/Hz	Turbulence-free	All key devices were commercially available
AiPT [31]	689.2 Gb/s	2.2 m	LP	5	1	18.1 bit/s/Hz	Emulated turbulence	All key devices were commercially available
USC [21]	400 Gb/s	1 m	HG/LG	4	1	≤8 bit/s/Hz	Turbulence-free	Bulk-optics multiplexer and demultiplexer
HUST [122]	80 Gb/s	260 m	OAM	2	1	≤8 bit/s/Hz	Field Demonstration	Bulk-optics multiplexer and demultiplexer
BUPT [49]	40 Gb/s	2 m	Gaussian	1	1	≤2 bit/s/Hz	Emulated turbulence	SIMO system using 3 LP modes for reception
NEC [126]	10 Gb/s	320 m	Gaussian	1	1	≤1 bit/s/Hz	Field Demonstration	SIMO system using 6 LP modes for reception
IT-Aveiro[127]	1 Tb/s	3 m	Gaussian	1	1	9.1 bit/s/Hz	Turbulence-free	w/ adaptive probabilistic constellation shaping
ETH [70]	1 Tb/s	53 km	Gaussian	1	1	≤11.9 bit/s/Hz	Field Demonstration	w/ AO for turbulence mitigation
DLR [128]	1.72 Tb/s	10.45 km	Gaussian	1	40	≤1 bit/s/Hz	Field Demonstration	OOK used
DLR [129]	13.16 Tb/s	10.45 km	Gaussian	1	54	≤8 bit/s/Hz	Field Demonstration	DP-QAM used
EC System [130]	30 Gb/s	1.3 km	Gaussian	1	3	Not reported	N/A	Commercial product
Collinear Networks [131]	10 Gb/s	Up to 5 km	Gaussian	1	1	Not reported	N/A	Commercial product

[a]The product of transmit mode count, wavelength count, symbol rate and bits per symbol.

Table 4
Challenging issues and possible solutions for high-capacity MDM-FSO implementation.

Issues	Causes	Possible solutions
Power limited	Absorption, scattering, turbulence, divergence, pointing error, insertion loss	High power laser, sensitive receiver, optical amplifier, more receive modes, ATP, relay, large receiver aperture, beam forming
Inter-mode crosstalk and MDL	Turbulence, divergence, pointing error, multiplexer/demultiplexer, multi-mode optical amplifier, incomplete modal overlap	Optimization of modes, AO, MIMO DSP, more receive modes, large receiver aperture, beam forming
Commercialization	N/A	Low-cost integration technologies, simplified MIMO DSP

lower than MDM-FSO systems. This indicates the great potential of MDM to overcome the "capacity crunch" of optical networks. Nevertheless, SISO-FSO systems have significant advantages over MDM-FSO systems in long-reach outdoor applications. It is because the FSO channel impairments such as turbulence and pointing errors not only cause power losses but also induce additional MDL and inter-mode crosstalk to an MDM-FSO signal, as we discussed earlier in Section 2.2. This makes MDM-FSO systems, especially when utilizing complete modal bases, much more sensitive to these impairments compared to a SISO-FSO system.

4. Discussions

In Table 4, we summarize the challenging issues and possible solutions for the implementation of high-capacity MDM-FSO systems leveraging complete modal base sets.

Similar to the communication over optical fibers and SISO-FSO links, one of the major limitations preventing MDM-FSO systems from achieving a higher data rate and longer transmission distance is the limited receive optical power. The causes of link losses could be the fundamental absorption and scattering effects, atmospheric turbulence, beam divergence, pointing error, and other insertion losses. This issue is more crucial for an MDM-FSO system since for a given launch power, less power is allocated to each transmit channel compared to a SISO-FSO system. A straightforward solution is increasing the launch power with a high-power laser or optical amplifier. However, in practical applications, we need to consider eye safety in the meanwhile. For example, in the International Electrotechnical Commission (IEC) standard, for light in the wavelength range from 1.4 μm to 4.0 μm, Class 1 products limit the accessible emission to 10 dBm (24.5 mm diameter area at a 2 m distance and 3.5 mm diameter area at a 100 mm distance) [133,134]. Another approach to enhance the performance is increasing the number of receive modes as we present earlier, at the expense of resources as well as cost. It should be noted that although compared to the SISO-FSO system, each mode has a lower received SNR for a given total signal power, the overall spectral efficiency can still increase by spreading the available power over more modes. For simplicity, we ignore the effects of inter-mode crosstalk. Then, the Shannon limit of an MDM system is [135–137]

$$C_{MDM} = N_t B \log 2 \left(1 + \frac{SNR}{N_t}\right), \tag{15}$$

where B is the bandwidth, SNR is corresponding to the SISO system (without MDM), and SNR/N_t is the mode-average SNR when there is no inter-mode crosstalk (i.e., $N_t = N_r$) or other mode-dependent impairments (e.g., MDL). From Fig. 19, we can see that for a given total received signal power, the overall spectral efficiency increases as the number of transmit modes increases. The result implies that we can still significantly increase the capacity of the FSO system by using as many modes as we can cost-effectively implement.

To deal with pointing errors, an ATP system is usually required, which is already employed in many commercial SISO-FSO products [130,131]. Besides, optical beam forming, also called beam shaping, is a promising solution to mitigate the effects of misalignments at a limited-size receiver. By emitting a single beam consisting of multiple specially designed complex-weighted spatial modes, this approach can reduce not only power losses but also crosstalk due to misalignment [138].

Different from SISO-FSO systems, the performance of MDM-FSO systems is also limited by the inter-mode crosstalk and MDL. There are various causes, including turbulence, divergence, pointing errors [139], MDM-related devices, and imperfect coupling from free space to fiber due to incomplete modal overlap [42]. Since the inter-mode crosstalk is

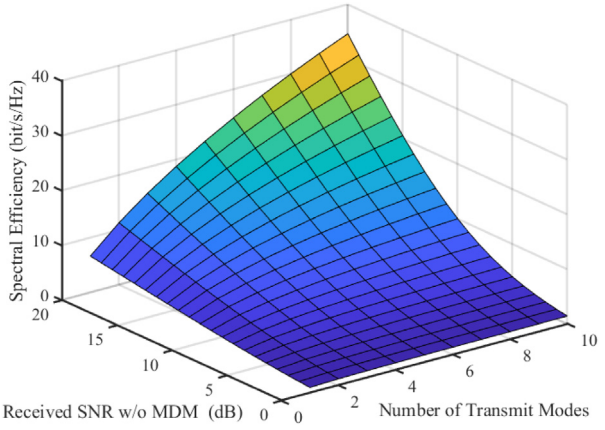

Fig. 19. Shannon limit of MDM systems without considering inter-mode crosstalk or any mode-dependent impairments.

stronger between two adjacent modes, an efficient solution to mitigate this kind of degradation is the optimization of modes for carrying data, which is more meaningful for the schemes utilizing complete modal basis sets. It is because they are more sensitive to these channel impairments. By dividing modes into different mode groups based on their indices, the mode-group division multiplexing can efficiently improve the performance compared to a simple MDM scheme, which has been verified for both the cases of fiber modes [140] and free-space modes [141].

As we discussed earlier, the scheme based on AO is an efficient approach that has been widely studied due to its ability to correct wavefront distortions caused by atmospheric turbulence [70,107,109,110]. It is particularly useful for the MDM-FSO systems in turbulence since the modal coupling can also be partially undone after the wavefront correction. However, an AO system will inevitably increase the hardware complexity, and cannot fully compensate for the effects of turbulence, leading to residual inter-mode crosstalk [109,110]. On the other hand, DSP is another powerful approach to mitigate turbulence effects, which can reduce the complexity in the optical domain. There have been many reported demonstrations using MIMO DSP to cancel the inter-mode crosstalk in an MDM-FSO system [14,31,80,142,143], including our schemes earlier presented in this paper. Nevertheless, MIMO DSP is also facing many challenges, e.g., scaling the number of modes for real-time implementation.

On the commercialization path of high-capacity MDM-FSO systems, both low-cost integration technologies and simplified MIMO DSP are desired. Many current MDM-FSO demonstrations are realized based on bulky, slow, and costly types of SLMs, which are not suitable as a practical solution for multiplexing and demultiplexing. Although there are already some commercial products of photonic lanterns [87] and MPLC [88], low-cost photonic integrated circuits are still desired to enable the commercial deployment of high-capacity MDM-FSO systems. Meanwhile, since complete modal basis sets are more sensitive to channel impairments such as turbulence and device-induced inter-mode crosstalk, MIMO DSP is usually required for the maximization of throughput. In this case, the capacity of MDM-FSO systems is limited by the size of the implementable MIMO DSP. For example, in a MIMO equalizer, its complexity is determined not only by the number of modes utilized but also by the tap size of the equalizer. A notable way to reduce the tap size required is to employ multicarrier modulation instead of single-carrier modulation [144]. Meanwhile, if we can minimize modal coupling effects, such as using beam forming and optimization of modes used, partial MIMO instead of full MIMO DSP is already sufficient to achieve decent performance [145]. At present, a real-time MIMO receiver prototype has been demonstrated to support 10 spatial modes in a weakly-coupled MDM system [146].

5. Conclusion

In this paper, we have summarized recent progress in MDM-FSO communications leveraging complete modal basis sets. Basic principles of spatial modes and channel impairments present in an MDM-FSO system have been discussed. Different from SISO-FSO systems, some impairments such as turbulence and pointing errors may also increase inter-mode crosstalk and MDL, degrading the performance of an MDM-FSO system. Meanwhile, the simulation results have shown that the tolerance to channel impairments of an MDM-FSO system is basis-dependent. We have then discussed different types of FSO systems and introduced a generalized MIMO FSO system supporting redundant receive modes, which can provide a compromise between transmission performance and requirements for resources. To further improve the robustness against FSO channel impairments, various solutions such as ATP mechanisms and MIMO DSP are required and have also been summarized. With the help of advanced DSP and a pair of commercial photonic lanterns, we have demonstrated record-high MDM-FSO single-wavelength transmission data rate as well as spectral efficiency in both scenarios without and with the effects of turbulence, while maintaining good practical applicability. Nevertheless, compared to the relatively mature SISO-FSO systems, there are still many challenging issues on the commercialization path of high-capacity MDM-FSO systems from both device and DSP perspectives.

Funding

This work was partly supported by EPSRC under grant numbers EP/T009047/1, EP/T009012/1, EP/S003436/1, and EP/S016171/1; European Union's Horizon 2020 research and innovation programme under the Marie Skłodowska-Curie grant agreement No. 713694 and under the Future and Emerging Technologies Open grant agreement Super-pixels No. 829116.

Declaration of competing interest

The authors declare the following financial interests/personal relationships which may be considered as potential competing interests: Aston University reports equipment, drugs, or supplies were provided by Ciena Corporation.

Data availability

The data that support part figures within this paper are available from Aston Data Explorer at https://doi.org/10.17036/researchdata.aston.ac.uk.00000540.

Acknowledgments

We would like to thank Ciena and Dr. Charles Laperle for kindly providing the WaveLogic 3 transponder used in our experiments.

References

[1] F. Tonini, et al., Cost-optimal deployment of a C-RAN with hybrid fiber/FSO fronthaul, IEEE/OSA J. Opt. Commun. Netw. 11 (7) (2019) 397–408.
[2] M.P.J. Lavery, et al., Tackling Africa's digital divide, Nat. Photon. 12 (2018) 249–252.
[3] A.S. Hamza, J.S. Deogun, D.R. Alexander, Classification framework for free space optical communication links and systems, IEEE Commun. Surveys Tuts. 21 (2) (2019) 1346–1382.
[4] A. Trichili, M.A. Cox, B.S. Ooi, M.-S. Alouini, Roadmap to free space optics, J. Opt. Soc. Amer. B 37 (11) (2020) 184–201.
[5] R.S. Kennedy, E.V. Hoversten, On the atmosphere as an optical communication channel, IEEE Trans. Inform. Theory IT-14 (5) (1968) 716725.
[6] E. Hoversten, R. Harger, S. Halme, Communication theory for the turbulent atmosphere, Proc. IEEE 58 (1970) 1626–1650.

[7] A. Belmonte, A. Comerón, J.A. Rubio, J. Bará, E. Fernández, Atmospheric-turbulence-induced power-fade statistics for a multi-aperture optical receiver, Appl. Opt. 36 (33) (1997) 8632–8638.

[8] X. Zhu, J. Kahn, Free-space optical communication through atmospheric turbulence channels, IEEE Trans. Commun. 50 (2003) 1293–1300.

[9] W. Popoola, Z. Ghassemlooy, J. Allen, E. Leitgeb, S. Gao, Freespace optical communication employing subcarrier modulation and spatial diversity in atmospheric turbulence channel, IET Opt. 2 (1) (2008) 16–23.

[10] F. Nadeem, V. Kvicera, M.S. Awan, E. Leitgeb, S.S. Muhammad, G. Kandus, Weather effects on hybrid FSO/RF communication link, IEEE J. Sel. Areas Commun. 27 (9) (2009) 1687–1697.

[11] P.J. Winzer, D.T. Neilson, A.R. Chraplyvy, Fiberoptic transmission and networking: The previous 20 and the next 20 years, Opt. Express 26 (18) (2018) 24190–24239.

[12] M. Ito, Space division multiplexed optical communication system including a pair of light responsive matrices, 1970, U.S. Patent No. 3, 492, 484.

[13] J. Wang, et al., Terabit free-space data transmission employing orbital angular momentum multiplexing, Nature Photon. 6 (7) (2012) 488–496.

[14] Y. Ren, et al., Free-space optical communications using orbital-angular-momentum multiplexing combined with MIMO-based spatial multiplexing, Opt. Lett. 40 (18) (2015) 4210–4213.

[15] A.E. Willner, et al., Optical communications using orbital angular momentum beams, Adv. Opt. Photonics 7 (1) (2015) 66–106.

[16] L. Li, et al., High-capacity free-space optical communications between a ground transmitter and a ground receiver via a UAV using multiplexing of multiple orbital-angular-momentum beams, Sci. Rep. 7 (1) (2017) 1–12.

[17] M.J. Padgett, Orbital angular momentum 25 years on [invited], Opt. Express 25 (10) (2017) 11265–11274.

[18] A. Trichili, et al., Communicating using spatial mode multiplexing: Potentials, challenges and perspectives, IEEE Commun. Surv. Tut. 21 (4) (2019) 3175–3203.

[19] A.E. Willner, et al., Recent advances in high-capacity free-space optical and radio-frequency communications using orbital angular momentum multiplexing, Philosoph. Trans. Roy. Soc. London A: Math. Phys. Eng. Sci. 375 (2087) (2017).

[20] N. Zhao, X. Li, G. Li, J.M. Kahn, Capacity limits of spatially multiplexed free-space communication, Nature Photon. 9 (12) (2015) 822–826.

[21] K. Pang, et al., 400-Gbit/s qpsk free-space optical communication link based on four-fold multiplexing of Hermite–Gaussian or Laguerre–Gaussian modes by varying both modal indices, Opt. Lett. 43 (16) (2018) 3889–3892.

[22] M.A. Cox, et al., The resilience of Hermite-and Laguerre- Gaussian modes in turbulence, J. Lightwave Technol. 37 (16) (2019) 3911–3917.

[23] M.A. Cox, N. Mphuthi, I. Nape, N.P. Mashaba, L. Cheng, A. Forbes, Structured light in turbulence, IEEE J. Sel. Top. Quantum. Electron. 27 (2) (2020) 7500521.

[24] L. Li, et al., Power loss mitigation of orbital-angular-momentum-multiplexed free-space optical links using nonzero radial index Laguerre– Gaussian beams, J. Opt. Soc. Amer. B 34 (1) (2017) 1–6.

[25] H. Song, et al., Demonstration of turbulence resilient self-coherent free-space optical communications using a pilot tone and an array of smaller photodiodes for bandwidth enhancement, in: Proc. OFC, San Diego, CA, USA, 2022, paper. M4I.4.

[26] S. Restuccia, D. Giovannini, G. Gibson, M. Padgett, Comparing the information capacity of Laguerre-Gaussian and Hermite-Gaussian modal sets in a finite-aperture system, Opt. Express 24 (24) (2016) 27127–27136.

[27] A. Trichili, et al., Optical communication beyond orbital angular momentum, Sci. Rep. 6 (2016) 27674.

[28] H. Huang, et al., 100 Tbit/s free-space data link enabled by three-dimensional multiplexing of orbital angular momentum, polarization, and wavelength, Opt. Lett. 39 (2) (2014) 197–200.

[29] Y. Ren, et al., Spatially multiplexed orbital-angular-momentum-encoded single photon and classical channels in a free-space optical communication link, Opt. Lett. 42 (23) (2017) 4881–4884.

[30] Z. Hu, et al., Single-wavelength transmission at 1.1-Tbit/s net data rate over a multimodal free-space optical link using commercial devices, Opt. Lett. 47 (14) (2022) 3495–3498.

[31] Y. Li, et al., Enhanced atmospheric turbulence resiliency with successive interference cancellation DSP in mode division multiplexing free-space optical links, J. Lightw. Technol. 40 (24) (2022) 7769–7778.

[32] A.E. Siegman, Lasers, Univ. Sci. Books, Sausalito, CA, USA, 1986.

[33] L. Allen, M.W. Beijersbergen, R.J.C. Spreeuw, J.P. Woerdman, Orbital angular momentum of light and the transformation of Laguerre–Gaussian laser modes, Phys. Rev. A 45 (11) (1992) 8185–8189.

[34] A.T. O'Neil, J. Courtial, Mode transformations in terms of the constituent Hermite-Gaussian or Laguerre-Gaussian modes and the variable phase mode converter, Opt. Commun. 181 (1–3) (2000) 35–45.

[35] D. McGloin, K. Dholakia, Bessel beams: Diffraction in a new light, Contemp. Phys. 46 (1) (2005) 15–28.

[36] J.C. Gutiérrez-Vega, M. Iturbe-Castillo, S. Chávez-Cerda, Alternative formulation for invariant optical fields: Mathieu beams, Opt. Lett. 25 (20) (2000) 1493–1495.

[37] M.A. Bandres, J.C. Gutiérrez-Vega, Ince–Gaussian beams, Opt. Lett. 29 (2) (2004) 144–146.

[38] R. Chen, H. Zhou, M. Moretti, X. Wang, J. Li, Orbital angular momentum waves: Generation, detection and emerging applications, IEEE Commun. Surv. Tut. 99 (1) (2019) 1–30.

[39] Z. Zhao, et al., Modal coupling and crosstalk due to turbulence and divergence on free space THz links using multiple orbital angular momentum beams, Sci. Rep. 11 (2021) 2110.

[40] A. Minoofar, et al., Experimental demonstration of sub-THz wireless communications using multiplexing of Laguerre-Gaussian beams when varying two different modal indices, J. Lightw. Technol. 40 (10) (2022) 3285–3292.

[41] A.E. Willner, et al., Perspectives on advances in high-capacity, free-space communications using multiplexing of orbital-angular-momentum beams, APL Photonics 6 (3) (2021) 030901.

[42] R. Brüning, Y. Zhang, M. McLaren, M. Duparré, A. Forbes, Overlap relation between free-space Laguerre Gaussian modes and step-index fiber modes, J. Opt. Soc. Amer. A 32 (9) (2015) 1678–1682.

[43] A.W. Snyder, J.D. Love, Optical Waveguide Theory, Chapman & Hall Press, London, U.K, 1983.

[44] A.A. Farid, S. Hranilovic, Outage capacity optimization for free-space optical links with pointing errors, J. Lightw. Technol. 25 (7) (2007) 1702–1710.

[45] M.P.J. Lavery, G.C.G. Berkhout, J. Courtial, M.J. Padgett, Measurement of the light orbital angular momentum spectrum using an optical geometric transformation, J. Opt. 13 (13) (2011) 064006–1–4.

[46] G. Xie, et al., Performance metrics and design considerations for a free-space optical orbital-angular-momentum-multiplexed communication link, Optica 2 (4) (2015) 357–365.

[47] J.C. Ricklin, F.M. Davidson, Atmospheric turbulence effects on a partially coherent Gaussian beam: Implications for free space laser communication, J. Opt. Soc. Amer. A, Opt. Image Sci. 19 (9) (2002) 1794–1802.

[48] B. Ndagano, N. Mphuthi, G. Milione, A. Forbes, Comparing mode-crosstalk and mode-dependent loss of laterally displaced orbital angular momentum and Hermite-Gaussian modes for free-space optical communication, Opt. Lett. 42 (20) (2017) 4175–4178.

[49] D. Zheng, et al., Performance enhancement of free-space optical communications under atmospheric turbulence using modes diversity coherent receipt, Opt. Express 26 (22) (2018) 28879–28890.

[50] P.J. Winzer, W.R. Leeb, Fiber coupling efficiency for random light and its applications to lidar, Opt. Lett. 23 (13) (1998) 986–988.

[51] D. Zheng, Y. Li, E. Chen, B. Li, D. Kong, W. Li, J. Wu, Free-space to few-mode-fiber coupling under atmospheric turbulence, Opt. Express 24 (16) (2016) 18739–18744.

[52] X. Zhong, Y. Zhao, G. Ren, S. He, Z. Wu, Influence of finite apertures on orthogonality and completeness of Laguerre-Gaussian beams, IEEE Access 6 (2018) 8742–8754.

[53] Y. Dikmelik, F.M. Davidson, Fiber-coupling efficiency for free-space optical communication through atmospheric turbulence, Appl. Opt. 44 (23) (2005) 4946–4952.

[54] Y. Chen, L. Tan, L. Zhao, J. Ma, The influence of alignment tolerance on coupling efficiency of FSOC system based on few-mode fiber, J. Opt. 22 (2020) 015602.

[55] Y. Bian, Y. Li, E. Chen, W. Li, X. Hong, J. Qiu, J. Wu, Free-space to single-mode fiber coupling efficiency with optical system aberration and fiber positioning error under atmospheric turbulence, J. Opt. 24 (2022) 025703.

[56] A.N. Kolmogorov, The local structure of turbulence in incompressible viscous fluid for very large Reynolds numbers, Dokl. Akad. Nauk SSSR 30 (4) (1941) 301–305.

[57] L.C. Andrews, R.L. Phillips, Laser Beam Propagation Through Random Media, second ed., SPIE, Bellingham, WA, USA, 2005.

[58] L.C. Andrews, R.L. Phillips, C.Y. Hopen, Laser Beam Scintillation with Applications, SPIE, Bellingham, WA, USA, 2001.

[59] D.L. Fried, Statistics of a geometric representation of wavefront distortion, J. Opt. Soc. Amer. 55 (11) (1965) 1427–1435.

[60] R.J. Noll, Zernike polynomials and atmospheric turbulence, J. Opt. Soc. America 66 (3) (1976) 207.

[61] J.A. Anguita, et al., Turbulence-induced channel crosstalk in an orbital angular momentum-multiplexed free-space optical link, Appl. Opt. 47 (13) (2008) 2414–2429.

[62] N. Chandrasekaran, J.H. Shapiro, Turbulence-induced crosstalk in multiple-spatial-mode optical communication, in: Proc. CLEO, San Jose, CA, 2012, Paper CF3I.6.

[63] T. Doster, A.T. Watnik, Laguerre–Gauss and Bessel–Gauss beams propagation through turbulence: Analysis of channel efficiency, Appl. Opt. 55 (36) (2016) 10239–10246.

[64] V.P. Aksenov, V.V. Kolosov, G.A. Filimonov, C.E. Pogutsa, Orbital angular momentum of a laser beam in a turbulent medium: Preservation of the average value and variance of fluctuations, J. Opt. 18 (5) (2016) 054013.

[65] M.A. Cox, C. Rosales-Guzmán, M.P. Lavery, D.J. Versfeld, A. Forbes, On the resilience of scalar and vector vortex modes in turbulence, Opt. Express 24 (16) (2016) 18105–18113.

[66] J. Wang, et al., N-dimensional multiplexing link with 1.036-Pbit/s transmission capacity and 112.6-bit/s/Hz spectral efficiency using OFDM-8QAM signals over 368 WDM pol-muxed 26 OAM modes, in: Proc. Eur. Conf. Opt. Commun, 2014, pp. 1–3.
[67] M. Arikawa, Y. Ono, T. Ito, Evaluation of blind diversity combining of severely faded signals for high-speed free-space optical communication under atmospheric turbulence, in: Proc. Eur. Conf. Opt. Commun, 2017, pp. 1–3.
[68] N.K. Fontaine, et al., Digital turbulence compensation of free space optical link with multimode optical amplifier, in: Proc. 45th Eur. Conf. Opt. Commun, Dublin, Ireland, 2019.
[69] M.A. Cox, L. Cheng, C. Rosales-Guzmán, A. Fobes, Modal diversity for robust free-space optical communications, Phys. Rev. A 10 (2) (2018) 024020.
[70] B.I. Bitachon, et al., Tbit/s single channel 53 km free-space optical transmission - assessing the feasibility of optical GEO-satellite feeder links, in: Proc. European Conference on Optical Communication, ECOC, 2022, paper Th3A.6.
[71] P. Gatt, T.P. Costello, D.A. Heimmermann, D.C. Castellanos, A.R. Weeks, C.M. Stickley, Coherent optical array receivers for the mitigation of atmospheric turbulence and speckle effects, Appl. Opt. 35 (30) (1996) 5999–6009.
[72] A. Belmonte, J.M. Kahn, Capacity of coherent free-space optical links using diversity-combining techniques, Opt. Express 17 (15) (2009) 12601–12611.
[73] S.M. Navidpour, M. Uysal, M. Kavehrad, BER performance of free-space optical transmission with spatial diversity, IEEE Trans. Wireless Commun. 6 (8) (2007) 2813–2819.
[74] N. Cvijetic, S.G. Wilson, M. Brandt-Pearce, Performance bounds for free-space optical MIMO systems with APD receivers in atmospheric turbulence, IEEE J. Sel. Areas Commun. 26 (3) (2008) 3–12.
[75] L. Li, et al., Demonstration of both mode and space diversity in a 100 Gbit/s QPSK free-space optical link to increase system tolerance to turbulence, in: Proc. OFC, 2019, paper. W4A.5.
[76] D. Tse, P. Viswanath, Fundamentals of Wireless Communication, Cambridge Univ. Press, Cambridge, U.K, 2005.
[77] K. Zou, et al., Demonstration of free-space 300-Gbit/s QPSK communications using both wavelength- and mode- division-multiplexing in the mid-IR, in: Proc Opt. Fiber Commun. Conf. Exhib, 2021, paper W7E.5.
[78] Y. Li, Z. Hu, D.M. Benton, A. Ali, M. Patel, A.D. Ellis, Demonstration of 10-channel mode-and polarization-division multiplexed free-space optical transmission with successive interference cancellation DSP, Opt. Lett. 47 (11) (2022) 2742–2745.
[79] Z. Hu, et al., Single-wavelength terabit multi-modal free space optical transmission with commercial transponder, in: Proc. ECOC, Basel, Switzerland, 2022, Paper Tu4F.5.
[80] Z. Hu, et al., Adaptive transceiver design for high capacity multi modal free-space optical communications with commercial devices and atmospheric turbulence, J. Lightw. Technol. (2023) http://dx.doi.org/10.1109/JLT.2023.3242215, early access.
[81] S. Cai, Z. Zhang, X. Chen, Turbulence-resistant all optical relaying based on few-mode EDFA in free-space optical systems, J. Lightw. Technol. 37 (9) (2019) 2042–2049.
[82] N. Fontaine, J. Carpenter, S. Gross, R.A. Correa, S.L. Saval, Y. Jung, Photonic lanterns, 3D waveguides, multiplane light conversion and other components that enable space division multiplexing, Proc. IEEE 110 (11) (2022) 1821–1834.
[83] R. Ryf, et al., Mode-division multiplexing over 96 km of few-mode fiber using coherent 6 × 6 MIMO processing, J. Lightw. Technol. 30 (4) (2012) 521–531.
[84] G. Labroille, P. Jian, N. Barré, B. Denolle, J.-F. Morizur, Mode selective 10-mode multiplexer based on multi-plane light conversion, in: Proc. Opt. Fiber Commun. Conf, 2016, pp. 1–3, Paper Th3E.5.
[85] M. Mirhosseini, O.S. Magaña-Loaiza, C. Chen, B. Rodenburg, M. Malik, R.W. Boyd, Rapid generation of light beams carrying orbital angular momentum, Opt. Express 21 (2013) 30196–30203.
[86] N. Fontaine, Components for space- division multiplexing, in: Proc. Eur. Conf. Opt. Comm, 2017, pp. 1–3.
[87] Multiplexer/demultiplexer Photonic Lantern [Online]. Available: http://www.phoenixphotonics.com/website/products/spatial_division_multiplexing_SDM_products.htm.
[88] PROTEUS-C [Online]. Available: https://www.cailabs.com/en/product/proteus-c/.
[89] S.G. Leon-Saval others, Mode-selective photonic lanterns for space-division multiplexing, Opt. Express 22 (1) (2014) 1036–1044.
[90] J.-F. Morizur, L. Nicholls, P. Jian, S. Armstrong, N. Treps, B. Hage, M. Hsu, W. Bowen, J. Janousek, H.-A. Bachor, Programmable unitary spatial mode manipulation, J. Opt. Soc. Amer. A 27 (11) (2010) 2524–2531.
[91] N.K. Fontaine, R. Ryf, H. Chen, D.T. Neilson, K. Kim, J. Carpenter, Laguerre-Gaussian mode sorter, Nat. Commun. 10 (1) (2019) 1865.
[92] G. Labroille, B. Denolle, P. Jian, P. Genevaux, N. Treps, J.-F. Morizur, Efficient and mode selective spatial mode multiplexer based on multi-plane light conversion, Opt. Express 22 (13) (2014) 15599–15607.
[93] N.K. Fontaine, et al., Hermite–Gaussian mode multiplexer supporting 1035 modes, in: Proc. Opt. Fiber Commun. Conf., OFC, Optical Society of America, Washington, DC, USA, 2021, pp. 1–3, Paper M3D-4.
[94] Z.S. Eznaveh, et al., Photonic lantern broadband orbital angular momentum mode multiplexer, Opt. Express 26 (23) (2018) 30042–30051.
[95] Y. Jung, et al., Cladding pumped few-mode EDFA for mode division multiplexed transmission, Opt. Express 22 (23) (2014) 29008–29013.
[96] J. Li, J. Du, L. Ma, M.-J. Li, K. Xu, Z. He, Second-order few-mode Raman amplifier for mode-division multiplexed optical communication systems, Opt. Express 25 (2) (2017) 810–820.
[97] H. Wen, et al., Invited article: Four-mode semiconductor optical amplifier, APL Photon. 1 (2016) 070801.
[98] D. Askarov, J.M. Kahn, Design of transmission fibers and doped fiber amplifiers for mode-division multiplexing, IEEE Photon. Technol. Lett. 24 (21) (2012) 1945–1948.
[99] G.L. Cocq, L. Bigot, A.L. Rouge, M. Bigot-Astruc, P. Sillard, Y. Quiquempois, Design and characterization of a multimode EDFA supporting 4 transverse mode groups for modal division multiplexed transmissions, in: Proc. Eur. Conf. Exhib. Opt. Commun, Amsterdam, The Netherlands, 2012, Paper Tu.3.F.4.
[100] Q. Kang, E.L. Lim, Y. Jung, J.K. Sahu, F. Poletti, C. Baskiotis, S. Alam, D.J. Richardson, Accurate modal gain control in a multimode erbium doped fiber amplifier incorporating ring doping and a simple LP01 pump configuration, Opt. Express 20 (2012) 20835–20843.
[101] P. Sillard, D. Molin, M. Bigot-Astruc, K. De Jongh, F. Achten, A.M. Velazquez-Benitez, R. Amezcua-Correa, C.M. Okonkwo, Low-differential-mode-group-delay 9-LP-mode fiber, J. Lightwave Technol. 34 (2) (2016) 425–430.
[102] G. Lopez-Galmiche, et al., Few-mode erbium-doped fiber amplifier with photonic lantern for pump spatial mode control, Opt. Lett. 41 (11) (2016) 2588–2591.
[103] R. Nasiri Mahalati, D. Askarov, J.M. Kahn, Adaptive modal gain equalization techniques in multi-mode erbium-doped fiber amplifiers, J. Lightw. Technol. 32 (11) (2014) 2133–2143.
[104] Y. Jung, et al., Cladding pumped few-mode EDFA for mode division multiplexed transmission, Opt. Express 22 (23) (2014) 29008–29013.
[105] Z.S. Eznaveh, N.K. Fontaine, H. Chen, J.E.A. Lopez, J.C.A. Zacarias, B. Huang, A.A. Correa, C. Gonnet, P. Sillard, G. Li, A. Schãlzgen, R. Ryf, R.A. Correa, Ultra-low DMG multimode EDFA, in: Proc. OFC, 2017, Paper. Th4A.4.
[106] Few Mode EDFA [Online]. Available: http://www.phoenixphotonics.com/website/products/Few_Mode_EDFA.htm.
[107] Y. Kaymak, et al., A survey on acquisition, tracking, and pointing mechanisms for mobile free-space optical communications, IEEE Commun. Surveys Tuts. 20 (2) (2018) 1104–1123, 2nd Quart.
[108] F.P. Guiomar, M.A. Fernandes, J.L. Nascimento, V. Rodrigues, P.P. Monteiro, Coherent free-space optical communications: Opportunities and challenges, J. Lightw. Technol. 40 (10) (2022) 3173–3186.
[109] Y. Ren, et al., Adaptive-optics-based simultaneous pre- and post-turbulence compensation of multiple orbital-angular-momentum beams in a bidirectional free-space optical link, Optica 1 (6) (2014) 376–382.
[110] X. Su, et al., Experimental demonstration of adaptive-optics-based turbulence mitigation in a mode-multiplexed free-space optical link by using both radial and Azimuthal spatial indices, in: Proc. OFC, 2022, paper M4I.2.
[111] N.K. Fontaine, et al., Space-division multiplexing and all-optical MIMO demultiplexing using a photonic integrated circuit, in: OFC 2012, 2012, paper PDP5B.1.
[112] R.G.H. van Uden, et al., MIMO equalization with adaptive step size for few-mode fiber transmission systems, Opt. Express 22 (1) (2013) 119–126.
[113] J.G. Proakis, M. Salehi, Digital Communications, fifth ed., McGraw-Hill, New York, 2008.
[114] G. Kulkarni, S. Adlakha, M. Srivastava, Subcarrier allocation and bit loading algorithms for OFDMA-based wireless networks, IEEE Trans. Mob. Comput. 4 (6) (2005) 652–662.
[115] P.S. Chow, J.M. Cioffi, J.A.C. Bingham, A practical discrete multitone transceiver loading algorithm for data transmission over spectrally shaped channels, IEEE Trans. Commun. 48 (1995) 772–775.
[116] B. Göhler, P. Lutzmann, Range accuracy of a gated-viewing system as a function of the number of averaged images, Electro Opt. Rem. Sens. Photonic Technol. Appl. 8542 (2012) 37–44.
[117] D.L. Fried, Time-delay-induced mean-square error in adaptive optics, J. Opt. Soc. Amer. A 7 (7) (1990) 1224–1225.
[118] M.T. Gruneisen, et al., Adaptive spatial filtering of daytime sky noise in a satellite quantum key distribution downlink receiver, Opt. Eng. 55 (2) (2016) 026104.
[119] H. Song, et al., Demonstration of using two aperture pairs combined with multiple-mode receivers and MIMO signal processing for enhanced tolerance to turbulence and misalignment in a 10 Gbit/s QPSK FSO link, Opt. Lett. 45 (2020) 3042–3045.
[120] D. Benton, et al., Emulating atmospheric turbulence effects on a micro-mirror array: Assessing the DMD for use with free-space-to-fibre optical connections, Eng. Res. Express. 4 (2022) 045004.
[121] L.M. Zhang, F.R. Kschischang, Staircase codes with 6% to 33% overhead, J. Lightw. Technol. 32 (10) (2014) 1999–2002.
[122] Y. Zhao, J. Liu, J. Du, S. Li, Y. Luo, A. Wang, L. Zhu, J. Wang, Experimental demonstration of 260-meter security free-space optical data transmission using 16 - *qam* carrying orbital angular momentum (*oam*) beams multiplexing, in: Proc. Optical Fiber Communication Conference, Optica Publishing Group, 2016, pp. Th1H–3.

[123] M. Krenn, et al., Twisted light transmission over 143 km, Proc. Nat. Acad. Sci. United States Amer. 113 (48) (2016) 13648–13653, 11.
[124] M.P.J. Lavery, et al., Free-space propagation of high-dimensional structured optical fields in an urban environment, Sci. Adv. 3 (10) (2017) e1700552.
[125] B. Rodenburg, et al., Simulating thick atmospheric turbulence in the lab with application to orbital angular momentum communication, New J. Phys. 16 (3) (2014) 033020.
[126] M. Arikawa, T. Ishikawa, K. Hosokawa, S. Takahashi, Y. Ono, T. Ito, Mitigation of fading caused by atmospheric turbulence with FMF coupling and maximum ratio combining used in 320-m free-space optical transmission of, in: Proc. Eur. Conf. Opt. Commun, Düsseldorf, Germany, 2016, Paper Th.2.P2.SC5.15.
[127] M.A. Fernandes, P.P. Monteiro, F.P. Guiomar, Single-wavelength terabit FSO channel for datacenter interconnects enabled by adaptive PCS, in: Proc. Opt. Fiber Commun. Conf. Exhibit, 2021, Art. no. Th5E.3.
[128] J. Poliak, R.M. Calvo, F. Rein, Demonstration. of, 1.72 Tbit/s optical data transmission under worst-case turbulence conditions for ground-to-geostationary satellite communications, IEEE Commun. Lett. 22 (9) (2018) 1818–1821.
[129] A. Dochhan, J. Poliak, J. Surof, M. Richerzhagen, H.F. Kelemu, R.M. Calvo, 13.16 Tbit/s free-space optical transmission over 10.45 km for geostationary satellite feeder-links, in: Proc. Photon. Netw.; 20th ITG-Symp, Leipzig, Germany, 2019, pp. 1–3.
[130] EL-30G [Online]. Available: http://www.ecsystem.cz/en/products/free-space-optic-equipment.
[131] LightCNX-510 SM [Online]. Available: https://www.collinear.com/lightcnx/.
[132] A. Ferrari, et al., Assessment on the achievable throughput of multi-band ITU-T G.652.D fiber transmission systems, J. Lightw. Technol. 38 (16) (2020) 4279–4291.
[133] IEC standard, Safety of laser products - part 1: Equipment classification and requirements, in: IEC-60825-1, 2014.
[134] K. Matsuda, M. Binkai, S. Koshikawa, T. Yoshida, H. Sano, Y. Konishi, N. Suzuki, Demonstration of a real-time 14 Tb/s multi-aperture transmit single-aperture receive FSO system with class 1 eye-safe transmit intensity, J. Lightw. Technol. 40 (5) (2022) 1494–1501.
[135] C.E. Shannon, A mathematical theory of communication, Bell Syst. Tech. J. 27 (1948) 379–423, 623–656.
[136] C.E. Shannon, W. Weaver, The Mathematical Theory of Communication, Univ. Illinois Press, Chicago, 1963.
[137] P.J. Winzer, G.J. Foschini, MIMO capacities and outage probabilities in spatially multiplexed optical transport systems, Opt. Express 19 (17) (2011) 16680–16696.
[138] K. Pang, et al., Experimental mitigation of the effects of the limited size aperture or misalignment by singular-value decomposition-based beam orthogonalization in a free-space optical link using Laguerre–Gaussian modes, Opt. Lett. 45 (22) (2020) 6310–6313.
[139] A.E. Willner, et al., Orbital angular momentum beams for high-capacity communications, J. Lightw. Technol. (2022) http://dx.doi.org/10.1109/JLT.2022.3230585, early access.
[140] J. Carpenter, B.C. Thomsen, T.D. Wilkinson, Degenerate mode-group division multiplexing, J. Lightwave Technol. 30 (24) (2012) 3946–3952.
[141] A. Wang, et al., Experimental demonstration of free-space orbital-angular-momentum mode-group multiplexing under atmosphere turbulence, in: Proc. Asia Communications and Photonics Conference, 2021, paper M5B.3.
[142] H. Huang, et al., Crosstalk mitigation in a free-space orbital angular momentum multiplexed communication link using 4 × 4 MIMO equalization, Opt. Lett. 39 (15) (2014) 4360–4363.
[143] Y. Ren, et al., Atmospheric turbulence mitigation in an OAM-based MIMO free-space optical link using spatial diversity combined with MIMO equalization, Opt. Lett. 41 (11) (2016) 2406–2409.
[144] K. Shibahara, et al., Dense SDM (12-core × 3-mode) transmission over 527 km with 33.2-ns mode-dispersion employing low-complexity parallel MIMO frequency-domain equalization, J. Lightw. Technol. 34 (1) (2016) 196–204.
[145] P. Sillard, et al., Few-mode fiber technology, deployments, and systems, Proc. IEEE 110 (11) (2022) 1804–1820.
[146] S. Beppu, et al., Weakly coupled 10-mode-division multiplexed transmission over 48-km few-mode fibers with real-time coherent MIMO receivers, Opt. Express 28 (13) (2020) 19655–19668.